AN EXPERIMENTAL STUDY OF PARTICLE-WALL COLLISION RELATING TO FLOW OF SOLID PARTICLES IN A FLUID

Thesis by

Michael Herbert McLaughlin

In Partial Fulfillment of the Requirements

For the Degree of

Mechanical Engineer

California Institute of Technology

Pasadena, California

1968

(Submitted May 17, 1968)

ACKNOWLEDGMENTS

Many people have made major contributions to this study. The author is particularly indebted to Professor Frank E. Marble who suggested the problem and directed the subsequent work. The author's committee, consisting of Professors Marble, W. D. Rannie, and J. K. Knowles, has provided sound guidance throughout his period of graduate study. Conversations with Professor E. E. Zukoski relative to this study and the experimental techniques employed were also valuable to the author.

During his program of graduate study, the author was supported through a NASA Traineeship. The experimental work was performed with the financial support of contract AF 33(615)-3785 with the Aeronautical Research Laboratory of the U. S. Air Force.

Notes of appreciation are due to Mr. Frank T. Linton for his advice on the design and fabrication of the experiment, Mr. Carl Eastvedt for his help with photographic problems, and to Mrs. Roberta Duffy for typing the manuscript. A final note of recognition is due to the author's family for providing the support and encouragement that enabled the work to be carried through to fruition.

ABSTRACT

A preliminary investigation was made into the momentum and energy losses resulting from particle collisions in a fluid with application to particle - fluid two-phase flows. In particular, the length scale over which these intereactions are important was investigated. The geometry chosen for the experiments was that of a sphere approaching an infinite wall, a geometry which tended to maximize the energy and momentum losses of the sphere.

The experiments were performed by dropping a steel sphere through a glycerin-water solution onto a steel surface. Flows for which the particle Reynolds number, Re_T (based on terminal velocity and particle diameter), ranged from 0.05 to 7870 were investigated by taking high-speed motion pictures. Position-time curves were generated, and it was shown that above a moderate Reynolds number the important momentum and energy interactions occurred within a fraction of a ball radius of the wall. As the Reynolds number was increased from the Stokes flow regime, the decrease of this interaction length was shown. At higher Re_T the viscous losses became an increasingly smaller per cent of the particle kinetic energy.

A preliminary investigation was made of an alternate test procedure utilizing a thin liquid film rather than the continuum tank. The results showed that a critical film thickness existed, above which the energy loss did not significantly increase with increasing film thickness. The prospects of correlating the continuum loss effects with the thin-film loss effects appeared good and warrant further investigation.

Photographic materials on pages 5 and 14 are essential and will not reproduce clearly on Xerox copies. Photographic copies should be ordered.

TABLE OF CONTENTS

LIST OF FIGURES

LIST OF TABLES

I. INTRODUCTION

The interest in particle - fluid two-phase flows has increased markedly over the past few years. Some of the important problems considered include accelerated flows in rocket exhausts containing metallic fuel components, the dust cooling techniques designed for nuclear reactors, and various fluidization processes.

A general review of the characteristics of particulate motion (particularly for a single particle) in a fluid stream was given by Torobin and Gauvin[1]. Hoglund[2] reviewed the progress in nozzle flow solutions in early 1962. Since then, Marble[3, 4] and Rannie[5] have introduced a linearized continuum analysis applicable, generally speaking, to flows in which the volume fraction occupied by the solid phase is small compared to one. A review of this technique with a discussion of results obtained from it and the limitations on its use was published by Marble in 1967[6]. Murray[7] presented some conjectures which may be applicable to flows with a high volume fraction of solid, as might be encountered in fluidization problems. No experimental foundation for considering particle-particle interactions exists for the analyses of either Marble or Murray.

The particular problem of interest here is a flow in which the particle - particle interactions have a significant effect on the momentum transfer in the flow. In early studies, this effect was shown to be negligible for certain flows with small concentrations of particles or with a limited size distribution so that collisions were infrequent. Marble[4] was able to introduce collisions under the assump-

tion that the momentum exchange between the particles was not significantly altered by the interactions of the particle flow fields. By comparing the time that two particles spend in their mutual flow fields to the time required for particle velocity disturbances to be damped out in Stokes flow (as a measure of the integrated effect of the forces involved), he was able to formulate the restriction for such flows as:

$$Re(\rho_s/\rho) \gg 1$$

with ρ_s and ρ being respectively the mass density of the material from which the particles were made and the local gas phase density, and Re being the Reynolds number based on the local gas properties, and the average radius and the relative velocity of the two interacting particles.

This restriction can be modified for flow regimes other than Stokes flow. In particular, at high Reynolds number, when the particle drag is proportional to the square of the velocity, the restriction reduces to:

$$(\rho_s/\rho) \gg 1 .$$

In order to relax this restriction, a more detailed description of the particle interactions must be obtained. This study represents a preliminary investigation into this problem, particularly with regard to the length scale over which the interactions affect the momentum transport in the flow field.

A preliminary analytic study was made utilizing an analysis similar to that employed in thin-film lubrication theory. The general characteristic of such flows is a high pressure gradient perpendicular to the line of approach of the particles, supported by the high shear

stresses resulting from the "squeezing" of the liquid film. The results indicated that the net particle - particle interaction effect came primarily from the period when the particles were within a fraction of a ball radius of each other. The experiment was designed to emphasize the loss of momentum and energy in this region.

The geometry chosen was a sphere approaching an infinite flat plate, an arrangement that accomplished the above objective and avoided the problems associated with trying to make two spheres collide along a given line of centers. Disregarding particle wake effects, this geometry would tend to overestimate the particle interaction distances, since the radial flow area available for the escape of the fluid between the two colliding bodies would be less for a sphere approaching a plane than for a sphere approaching another convex body.

II. TEST APPARATUS

Tank Apparatus

Figure 1 shows a view of the continuum test apparatus. The major components of this set-up include the test tank, the hardened steel anvil used as the rebounding surface, a plexiglass floor fitted flush with the anvil surface, and the electromagnetic drop mechanism.

The plexiglass tank was four feet high and had a 1-foot square cross section. The height was chosen to give a sufficient fall length so that the particles would reach their terminal velocities several inches above the 2-inch test zone directly above the anvil. The fall length required by a given particle in a given liquid to reach 99 per cent of its terminal velocity was estimated from an analysis by Moorman[8]. The depth of the test liquid and the placement of the drop mechanism were such that the total ball drop height was at least 1.5 times the estimated length required to reach 99 per cent of terminal velocity.

The rebounding surface was a hardened steel anvil, nominally 4 inches high, with a diameter of 4 inches. Its mass was greater than 2000 times the mass of the largest ball used. The complete anvil was given a "soft chrome" plating to reduce corrosion. The rebound surface was ground for smoothness and to remove the plating. A plexiglass ring glued to the tank floor located the anvil on the center axis of the tank.

The electromagnetic drop mechanism consisted of a 2500 (approximately) turn coil surrounding a 7/32-inch diameter mu-metal

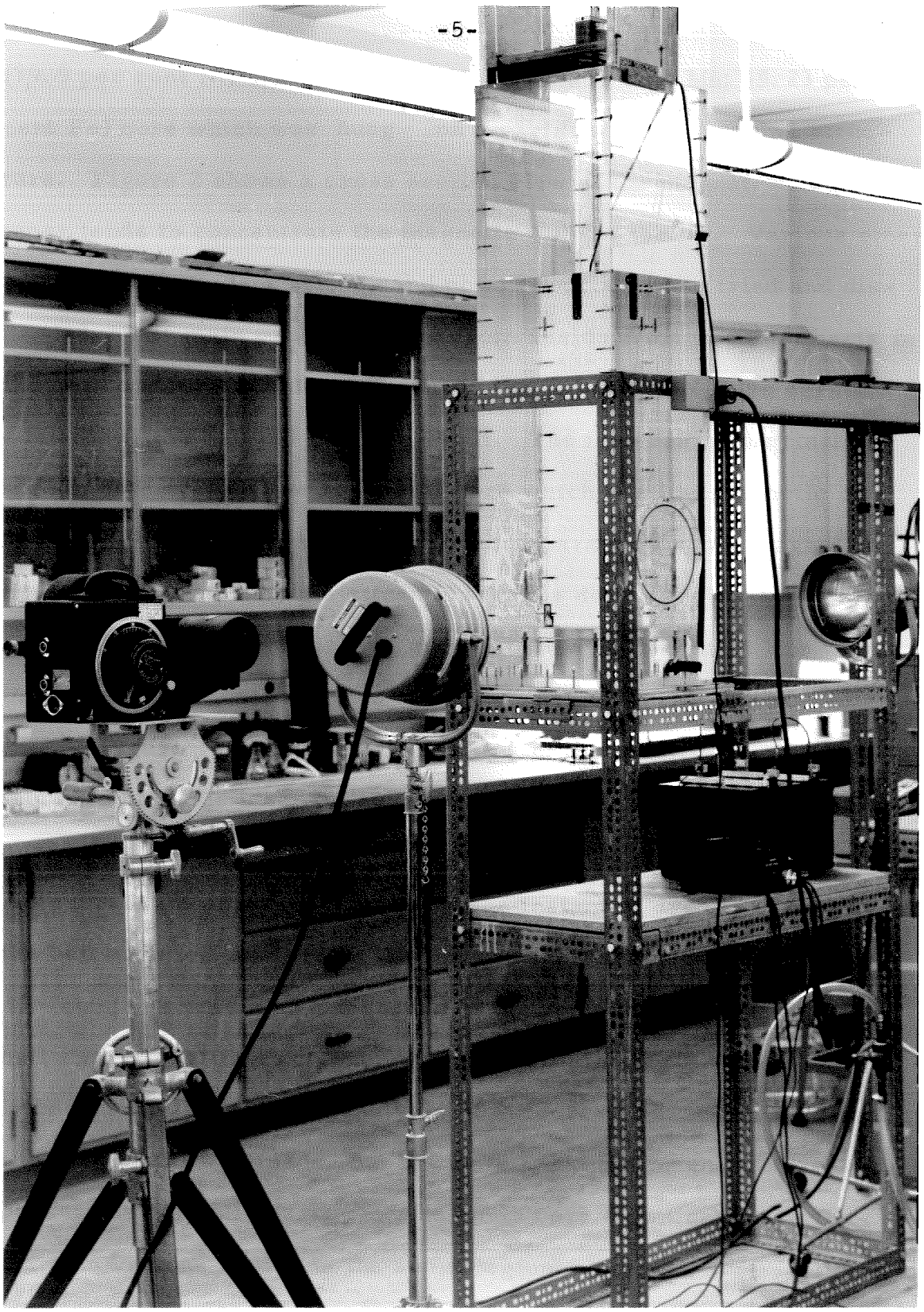

Figure 1. Continuum Test Tank and Apparatus

(79. 9 per cent Ni; 4. 77 per cent Mo ; 0. 10 per cent Mn; 15. 23 per cent Fe) core which was hung on a variable height support structure. Figure 2 shows a cross section view of the magnet. The core taper tends to concentrate the magnetic field at the tip. Various other core materials, geometries, and power sources were tried and discarded. The main problem arose from residual magnetism effects in the core and/or the balls that caused the drop control to be erratic; sometimes the ball did not drop at all. The features of the final design to note are: (1) the mu-metal core which has low magnetic retention; (2) the plastic tip insert which separates the two magnetic materials and lessens the attractive forces due to residual magnetism; (3) the DC-AC control circuit; and (4) the ball-tip contact line which minimizes rotational impulse of the drop.

Figure 3 is a schematic drawing of the electromagnet control circuit. The idea, as suggested by Moorman, was to use a DC current (of order 0. 1 amps) to provide the holding power and a small AC current (of order 10^{-4} amps) at the instant of drop to demagnetize the ball as it fell away from the tip. Rough tests using the deflection of a compass needle as a measure of the residual magnetism of the ball showed that this scheme, while not eliminating it, did significantly reduce it. No detailed analysis of the force interaction of the ball and steel anvil was made, but it was felt that the magnetic forces present as the ball approached the anvil were significantly smaller than the viscous forces in the same region.

Steel balls were chosen for the tests for several reasons:

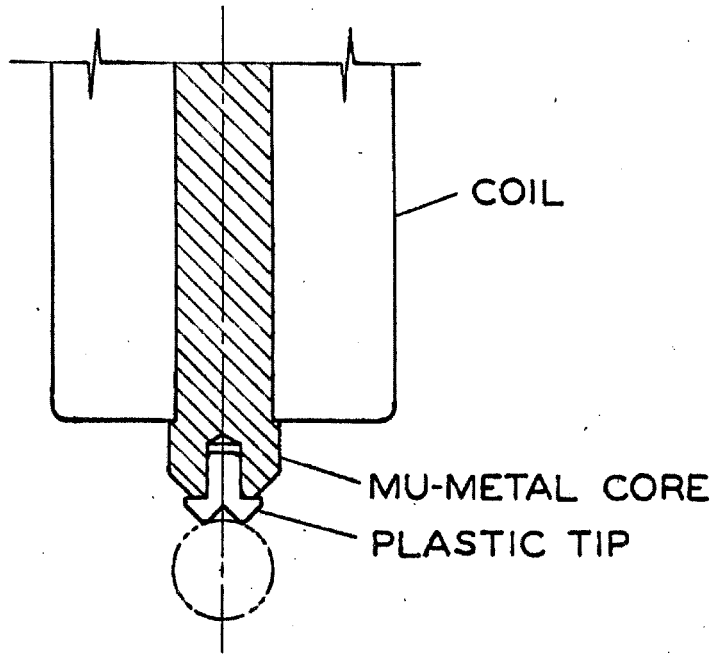

Figure 2. Cross Section View of Electromagnetic Drop Mechanism

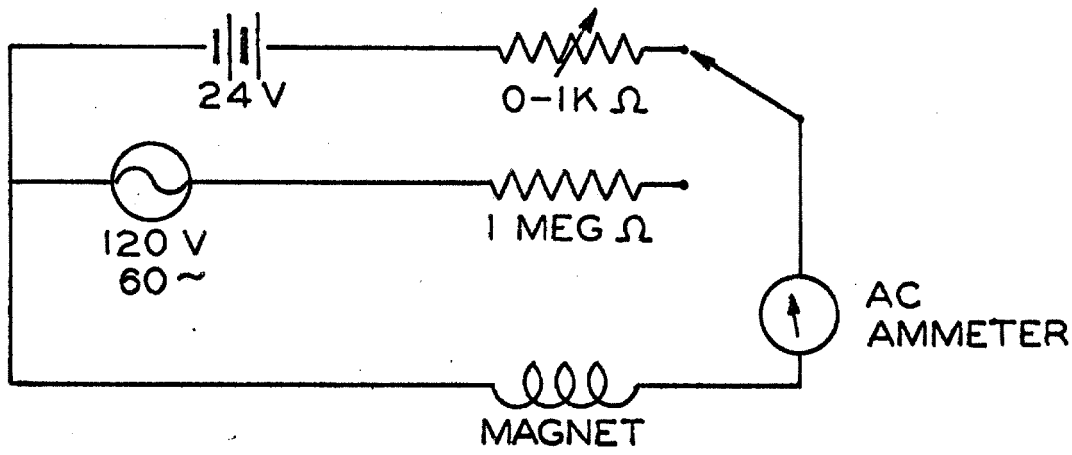

Figure 3. Electromagnet Control Circuit Shown in DC Power Position

(1) the density of the steel particles is significantly higher than the density of the liquids used, providing a greater kinetic energy at low Reynolds number flows; (2) the size and surface finish on steel balls can be rigidly controlled; (3) the use of steel particles impacting on a steel surface reduces the changes of significant surface chemistry effects; and (4) the magnetic properties permit the use of the electromagnetic drop system. The actual particles used were Grade 1 chrome steel balls manufactured by the Atlas Ball Division of SKF Industries, Inc. The tests incorporated balls of diameter range 3/32-inch to 3/8-inch. A value of 0.000025 inches is quoted by the manufacturer as the maximum diameter variation per ball. The sphericity is such as to give them an extremely "shiny" appearance.

U.S.P. Grade 99.5 per cent glycerin was chosen as the working fluid for these experiments for the following reasons: (1) using glycerin-water solutions, one could obtain the Reynolds number range required with moderate particle sizes; and (2) the properties of such solutions are available as a function of temperature and concentration. The major source of such information was a paper by Sheely[9], published in 1932. Data published by Bosart and Snoddy[10] were used to determine the variation of specific gravity with temperature.

The data from two preliminary test runs have also been included in this report. These tests (which are noted later) were run in tap water.

Test-tank temperatures were monitored by hanging two TCA

0^{o} - 50^{o}C total immersion thermometers in the tank on nylon fishing line. A typical positioning of the thermometers had one within an inch of the rebound surface and the other three inches from it. Both thermometers were hung approximately midway between the edge of the tank and the edge of the anvil. The maximum temperature differential registered (except for one case) was 0.2^{o}C. In light of the small differential, and in lieu of a more detailed analysis of the tank temperature distribution, the average of the two temperatures was used as the test temperature.

A detailed outline of the test procedure employed for the continuum test runs is contained in Appendix A.

Photographic Apparatus

The continuum test data were recorded on film by means of a 16-mm Kodak High-Speed Camera, using a 63-mm, f/2 Kodak Cine Ektar lens, both of which were manufactured by the Eastman Kodak Company. The camera was mounted on a heavy-duty Fastax tripod. The framing rate of the camera was adjustable within the range of approximately 1000 - 3500 frames per second. The instantaneous framing rate was determined from timing marker exposures placed on the film by a timing light built into the camera. A 1/4-watt lamp powered from 60-cycle line voltage produced exposures on the edge of the film at the rate of 120 per second.

Most of the preliminary test runs were filmed with a Hi-Cam movie camera with a top speed of 11,000 frames per second. For the preliminary test runs in water, the particle velocities were of the

order of 100 cm/sec, and the camera was run at 5000 frames per second. The quality of the filmed output was significantly higher using the Eastman camera, however, and the final experiments were designed to give sufficiently low velocities that the maximum framing rate of the Eastman would suffice.

Preliminary terminal velocity calculations for the test runs were utilized to set the framing speeds. Based on these preliminary data, the resolution, defined as the number of frames per ball diameter of fall, varied from 35 for the high-velocity runs to 100 for the low-velocity runs. The actual values varied somewhat from these preliminary values due to: (1) some runs occurring before the camera reached its full set speed; (2) the imprecise camera speed control; and (3) deviations from the velocities based on approximate fluid properties. The lowest resolution actually obtained was approximately 20. In many cases, the full resolution obtained was not required, and not all frames were processed for data.

One hundred foot rolls of Eastman Tri-X Negative film, type 7233, were used. This length roll gave a total run time (including acceleration) of $3\frac{1}{2}$ to 5 seconds for the framing rates used in the tests.

The intense light required at these high framing rates was provided by two flood lamps manufactured by Color Tran Industries and powered by a Cinemaster Chief Mark II transformer manufactured by the same company. It, in turn, was powered from a 220-volt power line, available in the laboratory. The lamps were run at an effective color temperature of 2950 - 3400^{o}K for the tests. The lights were

turned on immediately before the test was run and were shut off immediately after the test in order that there would be no significant effect on the tank temperature. Figure 4 shows the locations of the lights and the camera. A piece of translucent paper was placed over the back of the tank to provide diffuse back lighting. The lamp was positioned to give a uniformly lit background for at least 6 inches above the floor across the width of the anvil. The lower power front light provided an intense spot (or highlight) on the front of the ball. The combined lighting allowed several independent determinations of the ball position to be made.

Air Drop Experiments

Tests run to determine the energy loss associated with the anvil-ball interaction were run in air in a 12-inch wide by 11-inch deep wooden box with sliding plexiglass doors on the front and back. The sliding door on the back was spray-painted with flat black paint to reduce light reflection.

The same anvil, balls, and electromagnetic drop system used in the continuum tests were used here. In addition, a Graflex camera with Polaroid back was used to record the data. A strobe lamp provided the light source, oscillating at approximately 2000 cps, with the light-camera arrangement being the same as for the continuum tests, except that no back lighting was used.

The procedure used was to set the camera and strobe at the approximate anticipated rebound height (to reduce parallax error), drop the ball from the electromagnet, and open the camera shutter

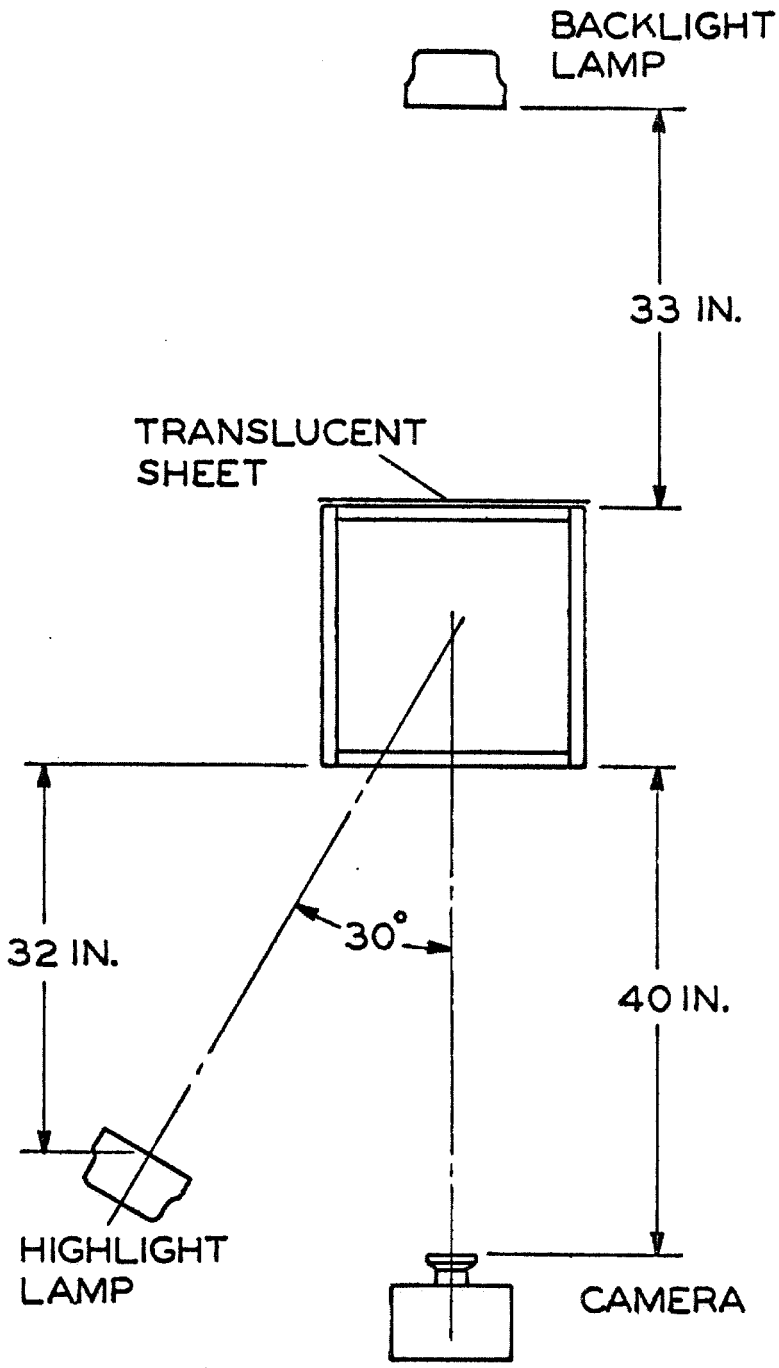

Figure 4. Location of Camera and Lights for Continuum Test Runs

for a long (several seconds) exposure. The result was a picture with a dotted trace of the ball path from which, using a toolmaker's microscope and a scale in the field of view of the camera, the rebound height could be established as a function of the initial height. Figure 5 shows a typical trace pattern. The field of view is centered at the anticipated rebound height and does not include the anvil surface.

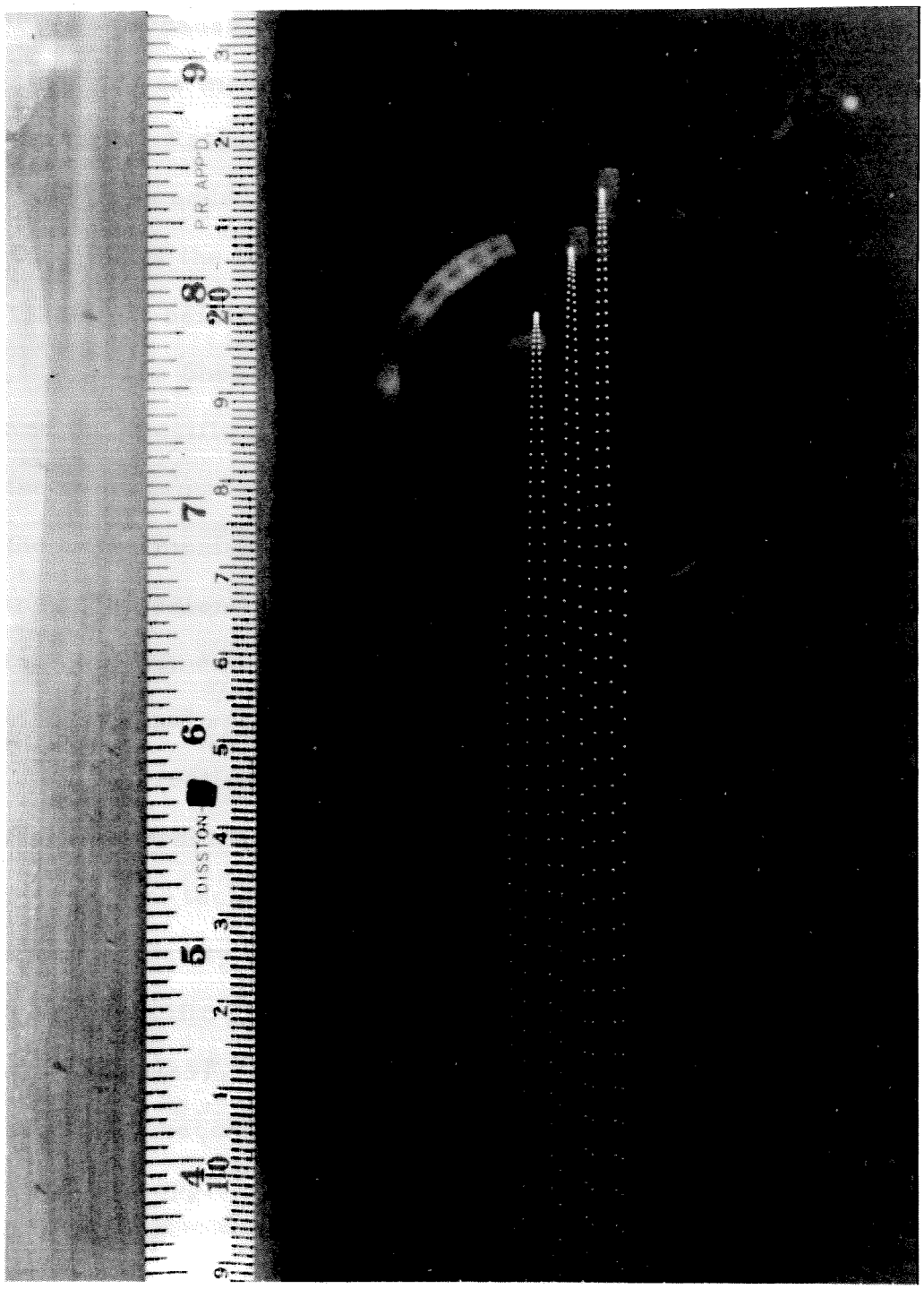

Figure 5. Typical Test Data Showing Ball Rebound for Dry Anvil Energy Loss Test Run

III. DETERMINATION OF PHYSICAL PROPERTIES

Because of the hygroscopic nature of the glycerin solution, no attempt was made to mix precise quantities of glycerin and water in the tank. Rather, an approximate calculation of the amount of each fluid to be added was done. The exact composition of the solution at the time of the test was determined by experiment from a sample taken just before the tests were run.

The Sheely data listed viscosity as a function of temperature and the specific gravity of the liquid at 25°C with respect to water at the same temperature [hereafter designated as sg(25/25)]. Thus, the experimental determination of viscosity and fluid density was most conveniently performed at 25°C. The test temperature for the tank experiments could not conveniently be held there. After the viscosity and specific gravity of each sample had been determined at 25°C, corrections were made to adjust these values to the measured test temperature.

Two techniques were used to determine the properties. The specific gravity was determined directly, using both a 25-ml and a 50-ml specific gravity bottle (pycnometer). From a plot of viscosity at 25°C, $\mu(25)$, as a function of sg(25/25), the viscosity was determined. A second experiment was performed to obtain the viscosity using a Hoeppler falling-ball viscosimeter as a check on the first. No attempt was made to recalibrate the viscosimeter. The manufacturer's empirical constants were used and the results used solely as a consistency check on the other technique. For detailed discussions

of the experimental procedures for these tests, see Appendix B.

The output from the viscosimeter test was the time, t , required for an appropriately chosen ball to traverse 100 mm along the length of a tube filled with the liquid at 25°C. The empirical fit used, after adjustment to the independent variable of interest sg(25/25), was

$$\mu(25) = K_1 t\{K_2 - sg(25/25)\} \ .$$

K_2 is a function of the density of the ball used, and K_1 is primarily a function of the clearance of the ball in the tube. A cross plot of this on the Sheely data gave the values of $\mu(25)$ and sg(25/25).

The direct outputs of the specific gravity measurements were the apparent masses of equal volumes of distilled water and the liquid of interest. All weighings were done on a single-pan precision balance in air. The individual weighings were those of the container (including enclosed air), the container plus water, and the container plus glycerin solution. To get a true value of the specific gravity, a correction had to be made for the trapped air included in the first weighing. A brief analysis showed that the change in the value of sg(25/25) was relatively insensitive to small errors in the correction mass. The value of the interior container volume was computed by dividing the apparent mass of water it held at 25°C by the density of water at that temperature. The density of dry air at 20°C (approximate temperature in room where the weighings were performed) was used. The mass correction added to the apparent weight of water and solution was 0.0611 gms for the 50 ml bottle and 0.0304 gms for the 25 ml

bottle.

Table 1 lists some of the quantities for the condition appropriate to test run 71.

TABLE 1. SPECIFIC GRAVITY DATA AND DERIVED QUANTITIES FOR RUN CONDITION E .

	25 ml bottle	50 ml bottle
apparent bottle weight, gm	24.5521	41.7069
weight of bottle plus solution, gm	55.2150	103.2452
weight of bottle plus water, gm	49.6366	92.0471
apparent solution weight, gm	30.6629	61.5383
apparent water weight, gm	25.0845	50.3402
corrected solution weight, gm	30.6933	61.5994
corrected water weight, gm	25.1149	50.4013
specific gravity, sg(25/25)	1.22212	1.22218

The time measured in the viscosimeter test for the liquid sample was 90.62 seconds, giving an empirical fit of:

$$\mu(25) = 11.844\,(7.8959 - sg(25/25)) .$$

Figure 6 shows the relationship of these independent determinations, and Table 2 lists the results for comparison.

TABLE 2. COMPARISON OF SPECIFIC GRAVITY DATA WITH VISCOSITY DATA.

Measurement	Specific Gravity	Viscosity
viscosity, cp.	80.05 [2]	79.05 [1]
sg(25/25)	1.22216 [1]	1.22187 [2]

[1] Measured

[2] From graph, Figure 6 .

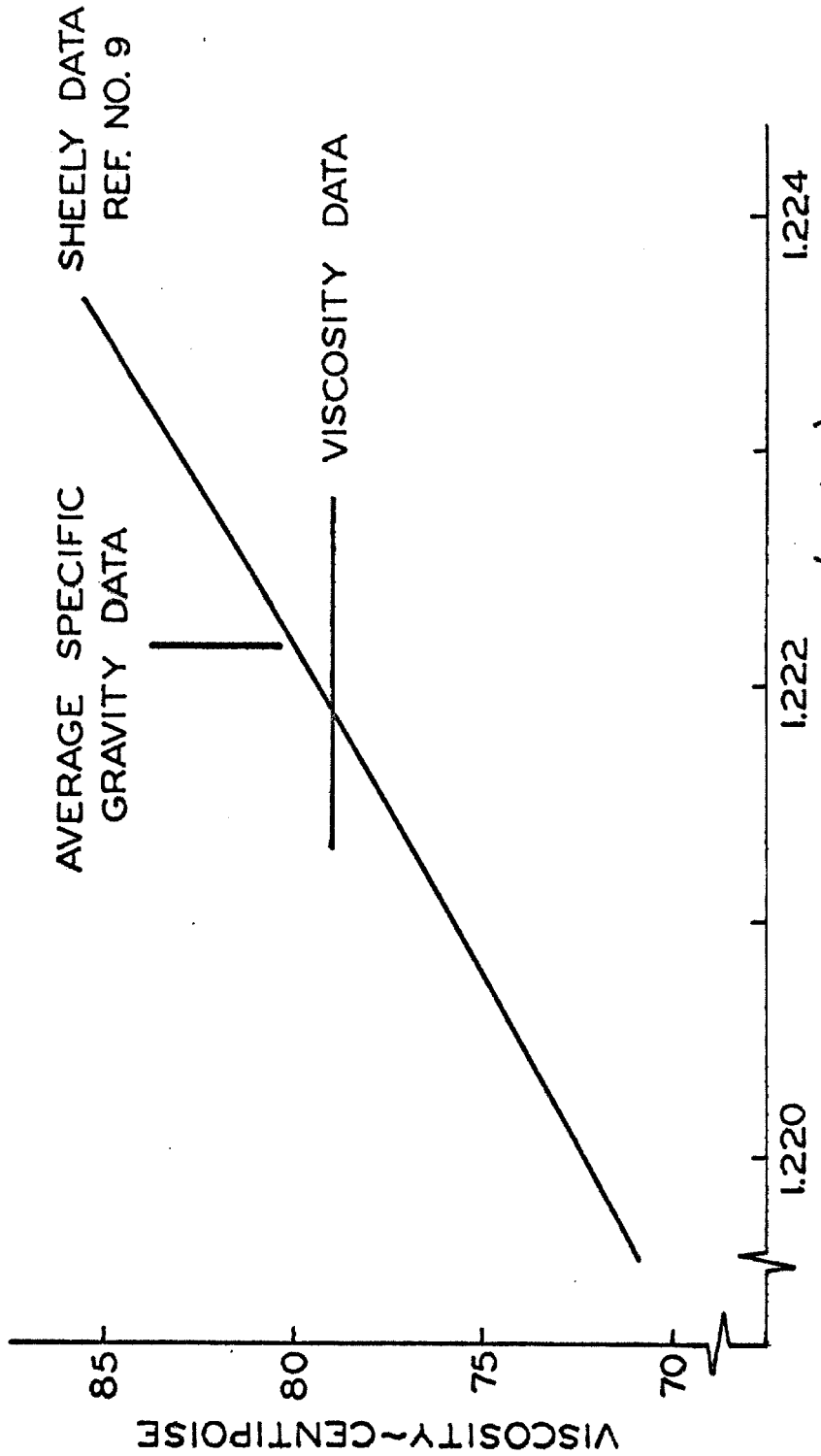

Figure 6. Comparison of the Independent Determinations of Viscosity and Specific Gravity for Run Condition E

The choice of readings was dictated by the consistency check. Various balls were used in the viscosimeter, depending on the range of viscosity being measured. With the high glycerin concentrations (conditions A and B), the two sets of readings agreed to within less than 1 per cent. After the ball was changed for the lower glycerin concentrations, the viscosity, as determined directly, fell consistently (1.25 - 3.3 per cent) lower than that determined by the specific gravity measurements. In all cases, the values determined by specific gravity measurement were used.

The next step was to determine the values of viscosity and fluid density at the test temperature T. The Sheely data give the viscosity for fixed concentrations at five temperatures between 20°C and 30°C. A plot was made of these data for the concentrations on either side of the test concentration. From the shape of these curves, the behavior of the curve for the intermediate test concentration was estimated, and the value of viscosity at the test temperature was read.

From the analysis of Bosart and Snoddy, a first order approximation to the temperature correction on the solution density was estimated to be:

$$\Delta\rho \cong 0.000615\,\{sg(25/25)\}\Delta T$$

for 80 per cent or more by weight glycerin solutions. The largest correction applied was + 0.00133 gm/cc.

Values for the density and viscosity of water (as required for preliminary test runs) were obtained from the Handbook of Chemistry and Physics[11]. A complete listing of test run physical properties and derived conditions is contained in Appendix C.

IV. DATA ANALYSIS

Timing Data

The data required to determine the time for each frame of interest was the location of the timing markers described in Part II. Forty frames of the film were considered as a unit. The length of the forty frames (nominally 12 inches) was measured to ± 0.01 inches using a scale. The length from the beginning of this forty-frame interval to each timing marker within the interval was then measured to the same accuracy. The number of frames after the start of the interval that each marker occurred was taken as the ratio of the marker measurement to the forty-frame measurement, times forty.

The absolute frame position was determined from this by arbitrarily choosing a position on the film to correspond to the origin of the frame numbering system. The absolute time was obtained by counting the timing markers from this arbitrarily chosen initial marker. No effort was made to make origin of the time correspond to the origin of the frame numbering system.

Two minor problems occurred using this technique. The edge of the timing markers to which the measurement had to be made tended to be fainter than the body of the marker, causing some uncertainty in locating the actual edge of the marker. A subjective judgement was required of the person taking the data. In addition, for the data occurring near the end of the roll, the chance of light-leak exposure of the extreme edges of the film increased. This caused a general blurring of the timing markers. In the latter case, the positions were lo-

cated as well as possible, and the plotted output of the timing computer program was examined. If necessary, the data in the blurred region were adjusted to give a smooth curve.

Figure 7 is a plot of this frame-time data for test run 71. The actual input data are recorded in Table 3.

TABLE 3. TIMING DATA FOR RUN 71.

I*	Location of Timing Blip in Frames
1	-2.64
2	16.69
3	35.34
4	55.05
5	74.04
6	94.02
7	113.10
8	133.38
9	152.87
10	173.38
11	193.10
12	213.98
13	233.93
14	255.09
15	275.20
16	296.52
17	316.98
18	338.63
19	359.21

* Time equals {(0.0083333)I} seconds.

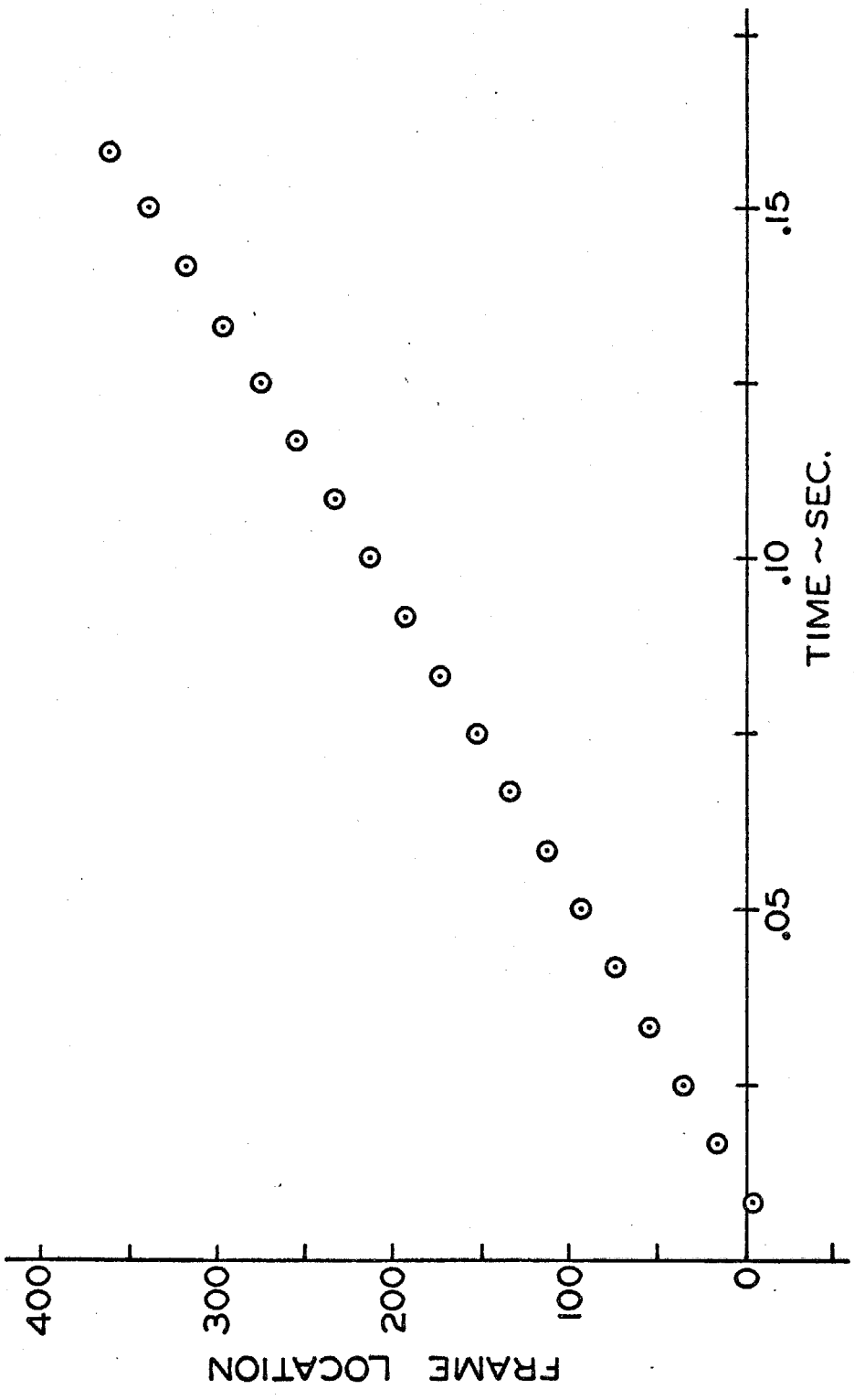

Figure 7. Timing Data for Run 71

The smooth appearance of the typical frame versus time data suggested that a low order polynomical would be sufficient to fit the data. A least squares polynomial fit subroutine was available in the CIT Subroutine Catalog. The data for each roll (time as a function of frame) were fit with polynomials of order two through six. The resulting fits were measured by computing the sum over the data of the square of the difference of computed time and experimentally determined time (hereafter referred to as CHISQR). The program outputs included the coefficients for each order of fit, the value of CHISQR, and a point plot of the input data as a check for errors.

When one attempted to fit the data with a higher order curve than was necessary to give a good fit, certain problems occurred during the inversion of matrices in the program. These problems resulted in no output for that order of fit.

Another problem occurred as a result of the magnitude of the data points. If time was fitted directly as a function of frame, the range of the independent variable would typically be 0 - 1000 , and that of the dependent variable would be 0 - 1 . This disparity in the size of the two variables leads again to matrix inversion problems. The solution was to rewrite the program with a scaled independent variable. The frame data were divided by 1000 , and time was fit as a function of this new variable.

Table 4 lists the CHISQR output for various order fits of the data of test run 71.

TABLE 4. MEASURE OF TIMING DATA FIT FOR RUN 71 .

Degree of Polynomial Fit	CHISQR
2	0.23554×10^{-6}
3	0.20283×10^{-6}
4 - 6	no fit

The criteria for choosing the order of fit took into account two considerations: (1) the order of the fit should be low in order that small, non-existent oscillations would not be present in the fit; and (2) CHISQR should be small. For the case illustrated, the improvement of the fit from order 2 to order 3 was not deemed significant, and the order 2 fit was used. The resulting fit was the following:

$$t = 0.950788 + 0.437764(N/1000) - 0.0665396(N/1000)^2 .$$

For fits involving a longer time interval with more data points, the CHISQR for the order 2 fit was generally two to three orders of magnitude higher than that for the run shown above. In all cases, CHISQR decreased as the order of the fit was increased, with an abrupt reduction of the rate of this decrease at some point. The criterion adopted was to choose the lowest order of fit such that increasing the order of fit by one did not result in a decrease of CHISQR by more than 30 - 40 per cent. This figure was not rigidly adhered to because the overall trend of the change in CHISQR was taken into account. The value of CHISQR for the chosen fits was typically $O(10^{-5} - 10^{-6})$ with a quadratic to quartic fit over thirty data points.

A check was made on this technique by comparing the resulting fits from two independent sets of timing marker data. The difference in computed times between the two fits was of order 10^{-5} seconds at selected points within the fit interval. Using the same set of data but comparing a CHISQR = 0.766×10^{-6} cubic fit with a CHISQR = 0.718×10^{-6} quartic fit, the difference was about 5×10^{-5} seconds near the edges of the interval and 1×10^{-5} in the central region.

Position Data

A major requirement for a study of this kind is an efficient technique for producing a large quantity of position data from the raw film. Figure 8 shows a schematic diagram of the equipment used in this study. A microfilm reader altered to handle 16-mm film was used to display the movie film. A cursor, supported by a spring-loaded pulley system and movable over the face of the microfilm reader by a handwheel, was the position-locating device. The handwheel was attached to the shaft of a Model C, 3-turn Helipot variable resistor, which acted as a voltage divider. A digital voltmeter provided a digital voltage output which was channeled to a keypunch machine for recording the data. The linearity of the resistor was estimated by the manufacturer to be 0.1 per cent. Since the error in locating the cursor was much more than this, it posed no problem.

The viewer projected the film approximately life-size. For a typical run with the system set for maximum sensitivity, the ratio of differential DVM output to an actual differential length in centimeters was approximately $\frac{1}{2}$.

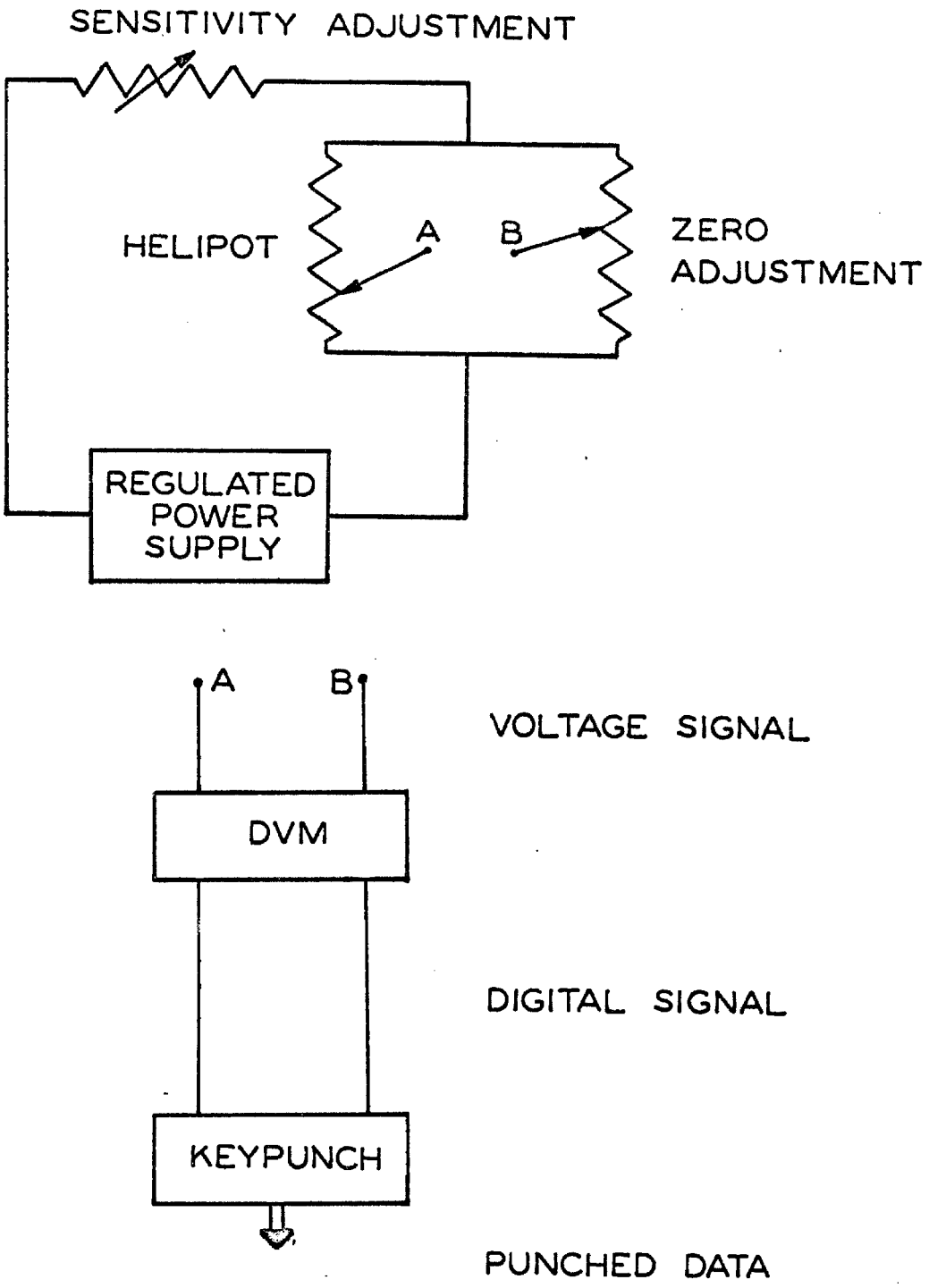

Figure 8. Schematic Diagram of Position Data Processing Equipment

Rather than trying to advance a given frame to an exact location on the viewer, the base or floor output reading was allowed to "float" within certain limits. The film position was allowed to vary to the extent that the floor reading, YF , was within ± 0. 100 DVM output units. While this introduced an extra data reading for each frame analyzed, it speeded up the entire process considerably because the locating time was significantly reduced.

Four position readings were taken for each frame; the floor, the bottom and top of the ball, and the highlight. Figure 9 shows the relationship of these readings as well as a set of typical readings. The quality of the filmed image of the floor line varied considerably. Several of the factors affecting this were: (1) light reflection from the floor surface; (2) the fact that the actual floor line seen was 6 inches closer to the camera than the focusing plane and was thus not in focus; and (3) camera alignment problems resulting in the floor plane not being perpendicular to the focusing plane,with the result that the back edge of the floor plane was also in view.

At one point during the preliminary testing, an alternate reference line was tried in order to avoid this problem. A piece of aluminum angle, approximately 1 inch wide with 2 inch legs, was machined flat on top and inserted in the focusing plane, off to the side of the anvil. Readings based on this reference showed more scatter than those based on the floor reading. The floor reading, although it did not always represent the "true floor," was adopted as the reference, and corrections were made to translate the resulting position

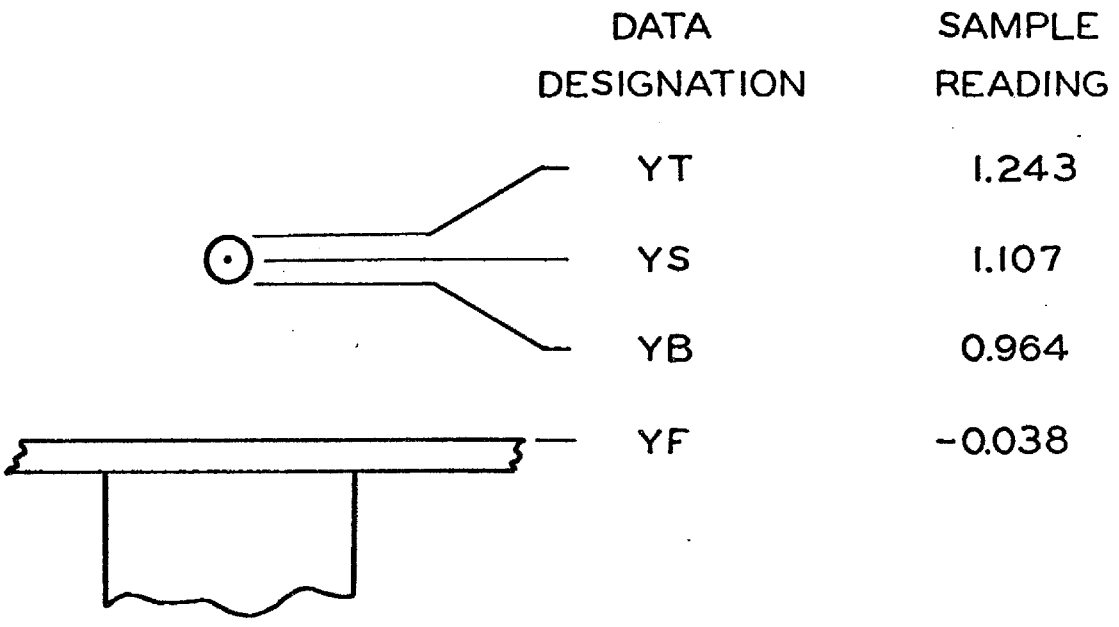

Figure 9. Identification of Position Readings with Sample Values

curves to a true zero-point.

Define the scale as being the ratio of differential height (in cm) to differential DVM output. Other variables introduced included:

$$XSF = (YS - YF)(\text{scale}) - R$$

$$XMF = \left[(YT + YB)/2\,(\text{scale})\right] - R$$

with R being the ball radius. Note that XSF represents the position of the bottom of the ball with respect to the floor based on the highlight measurement, and XMF is the same quantity based on the average position of the top and bottom of the ball. Other quantities were computed during the preliminary testing (based on the top of the ball reading with respect to floor, etc.), but XSF and XMF produced less scattered data more consistently.

Because of the use of a light source of finite extent to produce the highlight, it was impossible to do an exact analysis of the position of the highlight on the ball. The possibility of a significant position shift was reduced by the fact that only a 2-inch portion of vertical travel of the ball was used for data,coupled with the fact that both the camera and the light source were approximately 3 feet from the plane of the ball drop. A check was made during the computer analysis of the position data and showed that the ratio of XSF and XMF was close to 1 (within data scatter). No significant trend that would indicate a shifting of the highlight was noted.

The success of this method rested on the fact that errors in the position determination are random and can be overcome by analyzing enough frames. The major error was inpositioning the cursor

for the various readings. A measure of this error was computed by taking ten separate sets of data for two different frames. The data were taken at approximately the same operating speed as the actual run data. Figure 10 is a schematic of the two frames analyzed, and Table 5 lists the scatter as characterized by the sample standard deviation (small sample form)[12] for the readings and the differences of the readings. Remembering that these data in DVM output units must be multiplied by a scale factor of approximately 2, it is evident that we are talking about errors of the order of several hundredths of a centimeter. This error effectively limits the resolution possible by this technique. As the attempted resolution is increased, the error would become much larger than the frame-to-frame displacement of the ball, and the greater number of frames would not yield any further information.

TABLE 5. ERROR ANALYSIS DATA FOR TWO SAMPLE FRAMES

Reading	Mean for 10 Readings	Sample Standard Deviation
1	0.0707	0.0099
2	1.5327	0.0087
3	-0.1097	0.0098
4	0.0760	0.0062
(2)-(1)	1.4620	0.0143
(4)-(3)	0.1857	0.0133

Several techniques for establishing the length scale in the motion pictures were considered and tried. The idea of using a fiducial scale was discarded during the preliminary testing when, for 1/4-

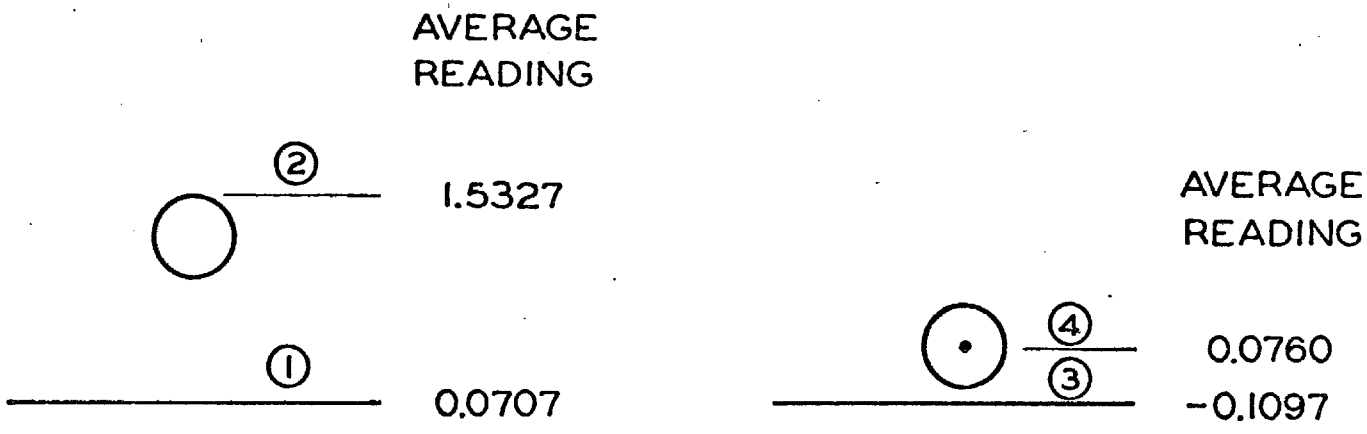

Figure 10. Schematic Diagram of Ball Positions for Frames Chosen for Error Analysis

inch balls dropped in pure water, the drop plane (with respect to the camera lens) could only be controlled to ± 3/4 inch. This led to a possible scale error on the order of 1 per cent. The problem of locating the floor (as discussed previously) would also introduce considerable error. Finally, the use of a fiducial scale would require another data point for each frame analyzed.

As the quality of the pictures improved during the testing period, the idea was developed to use the apparent diameter of the ball averaged over the frames as the reference scale. This method had the advantages of using an object in the correct plane, and if the data around the impact point were excluded, of using an object not subject to distortion near the floor plane. If the ball had a small velocity perpendicular to the lens axis, this method would tend to average the scale over the depth of the fall path. The major disadvantage of this technique was the possibility of light leakage, resulting in blurred edges from the strong back lighting. There was no problem of this kind for the larger balls (3/16-inch diameter and larger); and for the smaller balls, the intensity of the back lighting was reduced to lessen this effect.

The exact technique used to compute the scale is discussed in detail later in this section.

Position Data Analysis

The raw position data, obtained in the manner just described, were processed and analyzed by a series of three programs. For the initial program, PRM , the inputs were the ball diameter, the raw

position data, and the timing fit coefficients that were previously generated. After first computing a primary scale based on all of the input data, the program generated the values of time, XMF , XSF , XSF/XMF , and the apparent diameter of the ball for each frame of input. The values of apparent ball diameter and XSF/XMF were plotted as a function of frame, and XSF and XMF were plotted as a function of time. The latter plots gave a quick check on the quality of the data. The plot of the ratio of the two computed heights was used to check the consistency of the two methods and generally showed a very small deviation from 1.0 except during the time when the ball was near the plate and the data scatter became comparable to the position values.

As mentioned previously, the bottom edge of the ball became obscured when the ball approached the plate. The plotted output of apparent diameter as a function of frame was utilized to exclude this distortion from the computation of the scale.

A method was developed (program SCL) to process the remaining data to obtain a better approximation to the true scale. A new mean was computed; call it $\bar{D}(1)$. The data were reprocessed and all values of apparent diameter (XDIA) outside the range $(1.00 \pm 0.48)\bar{D}(1)$ were excluded from the computation of the new mean, $\bar{D}(2)$. The mean was iterated with smaller and smaller limits. The upper limit for the n^{th} iteration was $\bar{D}(n-1)[(1.04)^{12-n}]$, and the midpoint of the interval was $\bar{D}(n-1)$.

The complete set of data for run 71 was considered usable, there being no apparent distortion near the bounce point. Table 6

TABLE 6. SCL PROGRAM OUTPUT FOR RUN 71

Iteration	Factor	Number of Cards Included	Scale
	∞	198	2.0776676
1	1.480244	198	2.0776676
2	1.423312	197	2.0732040
3	1.368569	197	2.0732040
4	1.314932	197	2.0732040
5	1.265319	196	2.0765493
6	1.216653	195	2.0788922
7	1.169859	194	2.0768786
8	1.124864	191	2.0745964
9	1.081600	186	2.0731246*
10	1.040000	133	2.0667849

* Scale chosen.

shows the factor that multiplied $\bar{D}(n-1)$ to obtain the upper limit of the interval, the number of cards within the interval, and the value of the mean after each iteration for this run.

The data for this run were nicely clustered. The number of cards rejected does not become excessive until the final iteration. Twelve cards were rejected during the first 9 iterations, and 53 more were rejected during the last one. This fact, along with the appearance of the data, suggested using $\bar{D}(10)$ as the scale factor.

To show the effect of the sample chosen, the same analysis was run on the first 110 cards of the deck for run 71. This excluded all data in the impact and rebound time interval. Table 7 shows the computed values. The rejection factor is the same as listed in Table 6 for each iteration.

TABLE 7. SCL PROGRAM OUTPUT FOR RUN 71 USING PARTIAL SET OF DATA

Iteration	Number of Cards Included	Scale
	110	2. 1100175
1	110	2. 1100175
2	110	2. 1100175
3	109	2. 1020110
4	109	2. 1020110
5	109	2. 1020110
6	108	2. 1065894
7	107	2. 1031051
8	105	2. 1027821
9	101	2. 1028563 *
10	70	2. 1057373

* Scale chosen.

The difference of scale between the two is about 1. 5 per cent. Since the rebound velocity is important in this study, it was felt that the mean based on the full time interval would be appropriate, although it probably represented an "average" scale over the full time interval.

From the preliminary position plots, the amount that the reference plane differed from the true low-point position of the ball was obtained. Since it was based on the incorrect preliminary scale calculation, this value had to be corrected to the true scale value. The raw data were then reprocessed (program HGP) to yield plots of XMF and XSF corrected for scale and reference height. Punched and printed output of time, XMF , XSF , apparent diameter, and (XSF + 1)/(XMF + 1) were also generated. Figure 11 shows a cor-

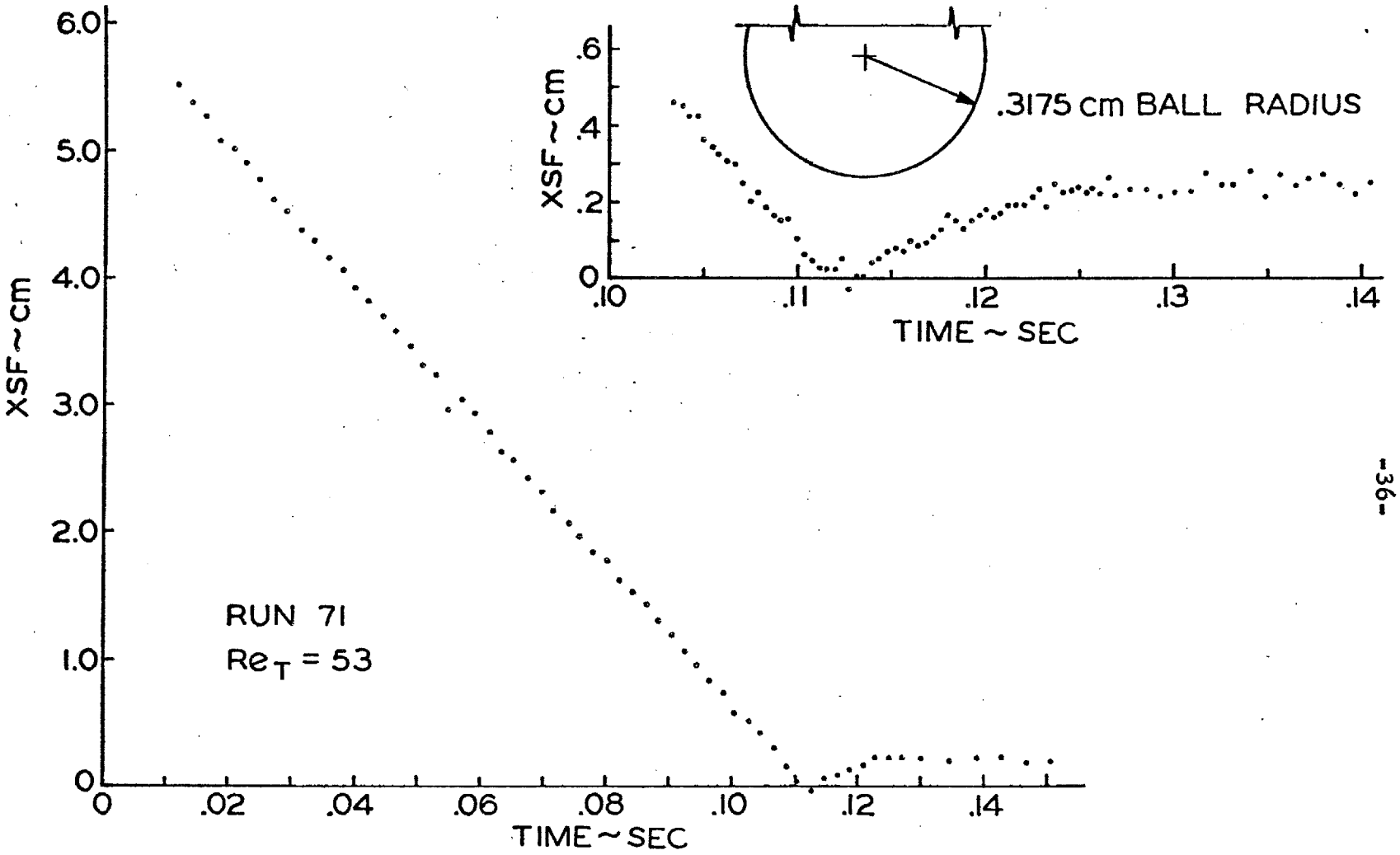

Figure 11. XSF Position Data for Run 71 Corrected for True Scale and Zero Reference

rected plot of XSF as a function of time for run 71. For this test run, every fifth frame was analyzed during the early portion of the run; every frame during the impact period; and every tenth frame during the late stages of the rebound period. On the main curve of Figure 11, every fifth frame is plotted where available. The insert shows the actual resolution with respect to the size of the ball with all frames included.

V. RESULTS

The primary output from the data analysis was the set of position-time curves corrected for true scale and zero-position. Figures 12(a-d) present selected runs over a Reynolds number range of 0.055 - 7870. As a check for reproducibility, Figure 13 shows a comparison of two separate runs (21 and 22) for the same test condition, and a comparison for run 22 of the highlight data (XSF) and the apparent ball midpoint data (XMF). No experiments were tried over a significant range of the ratio of particle density to fluid density (ρ_s/ρ). Thus, the effect of the density ratio on the scaling for the problem has not been verified. For this reason, all subsequent results will be presented as a function of Re_T, the terminal particle Reynolds number.

The most obvious characteristic of the position-time profiles was the change of the profile with increasing Re_T. The change in the profile occurred in two distinct Reynolds number regimes. For Re_T less than approximately 20, the particle kinetic energy was dissipated and there was no rebound from the plate; above this Reynolds number, the ball rebounded from the plate at some fraction of its incoming velocity. The higher Reynolds number regime was also characterized by the fact that within the experimental resolution, the ball hit the floor at terminal velocity (recall Figure 11 in Part IV). This suggests an energy loss mechanism with a very short length scale.

For problems in which the above-mentioned density ratio is nearly equal, one would suspect direct Reynolds number correlation. This is reinforced by the similarity of the profiles in Figure 14. The

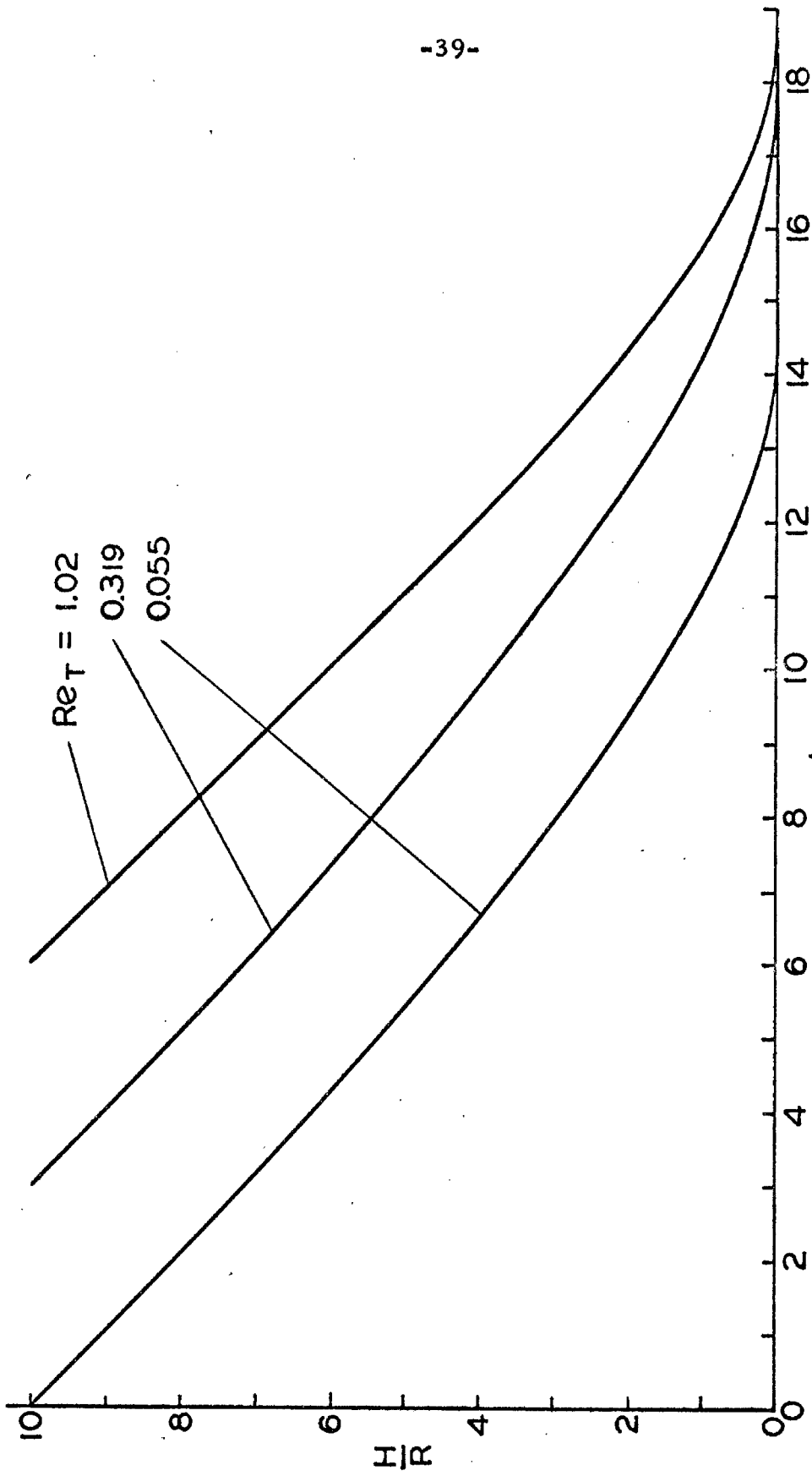

Figure 12(a). Position-Time Profiles for Selected Test Runs

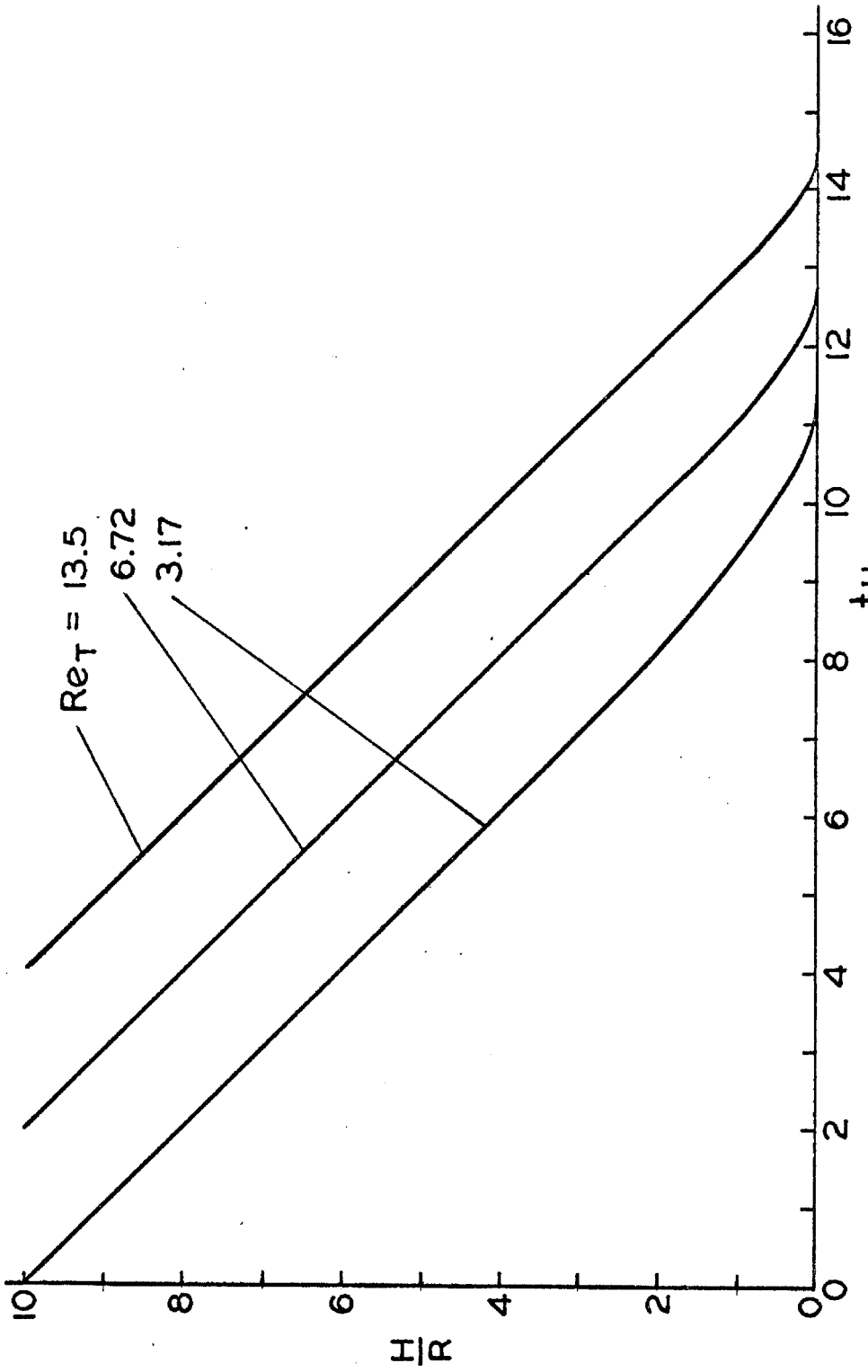

Figure 12(b). Position-Time Profiles for Selected Test Runs

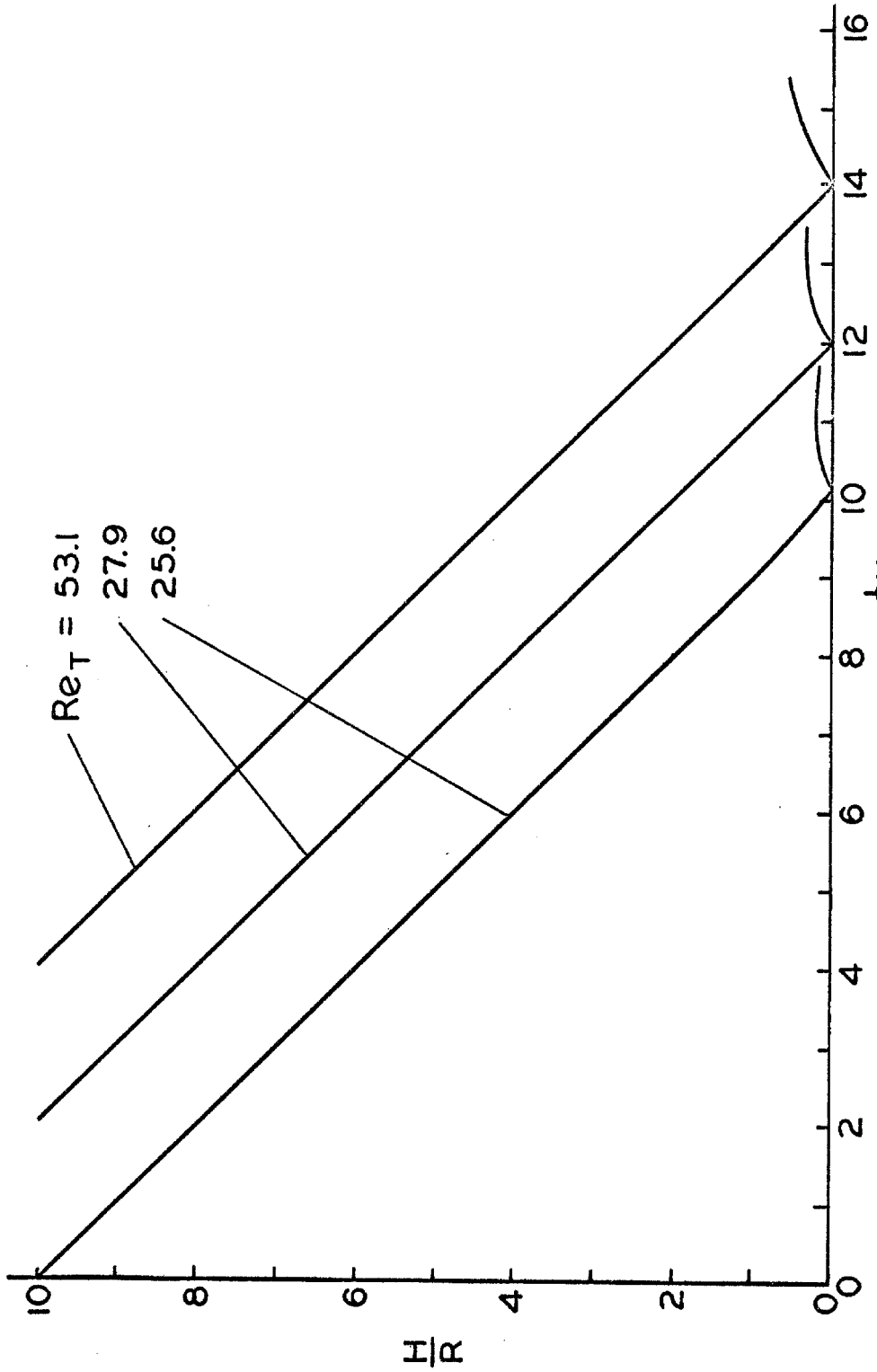

Figure 12(c). Position-Time Profiles for Selected Test Runs

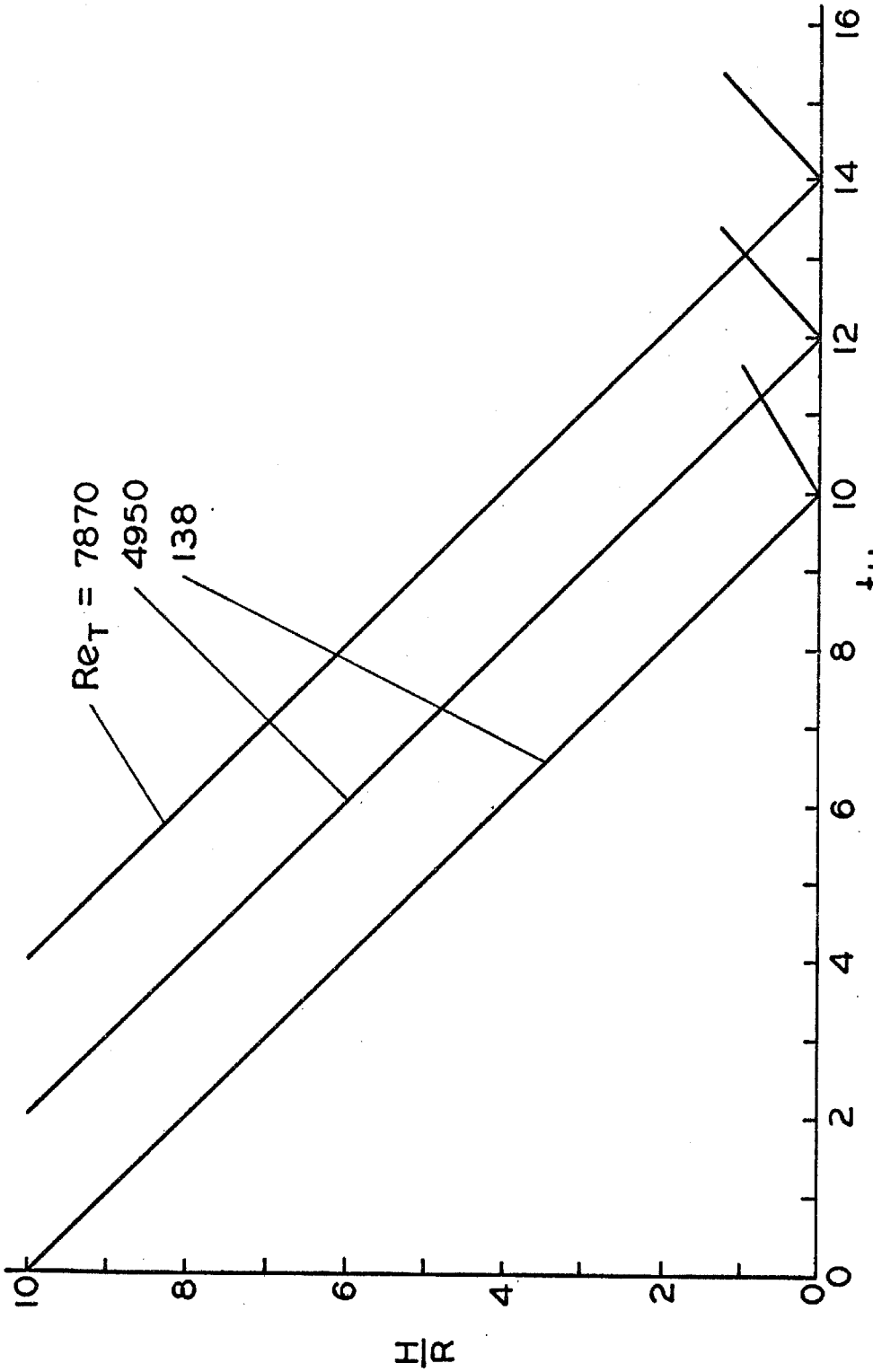

Figure 12(d). Position-Time Profiles for Selected Test Runs

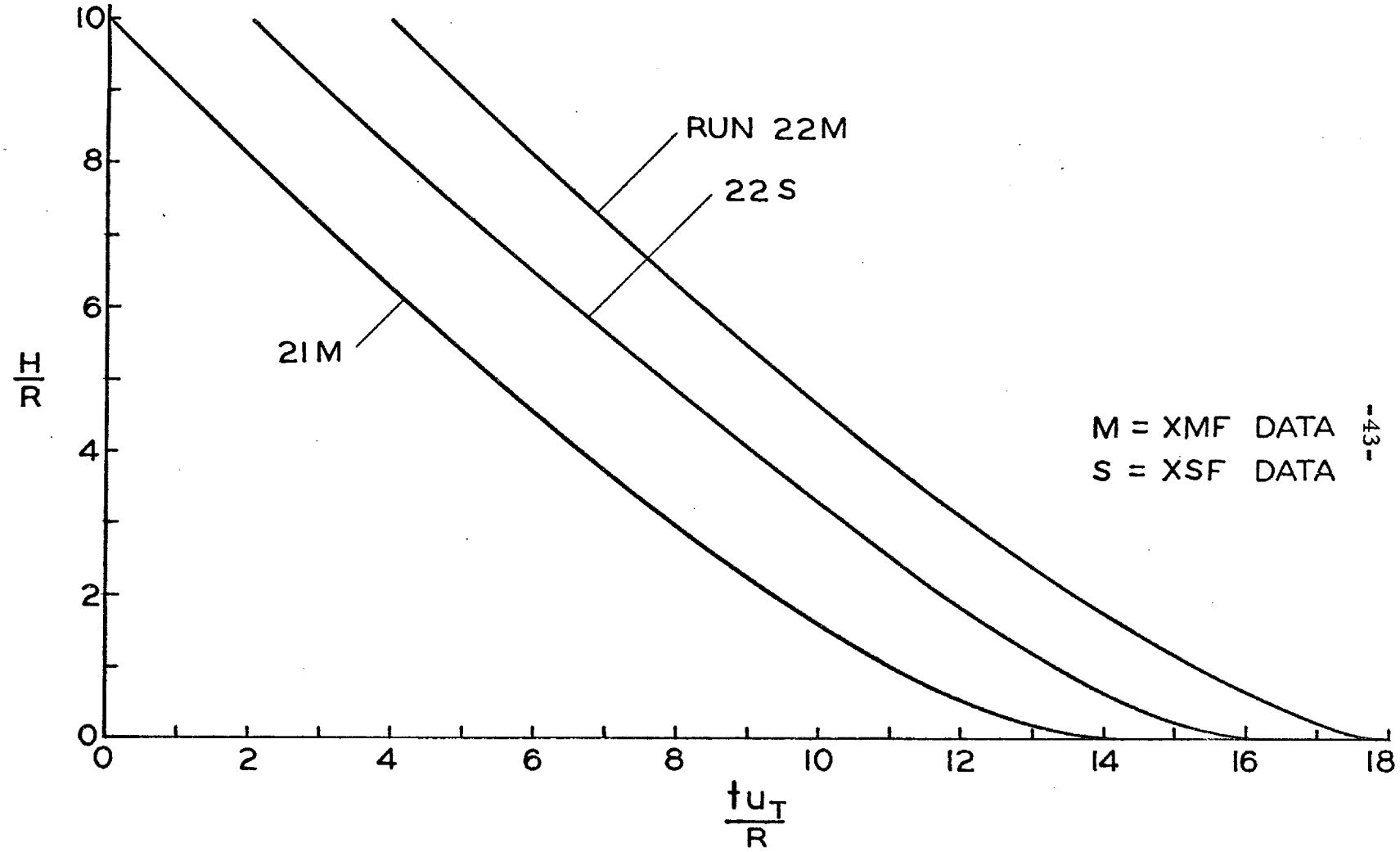

Figure 13. Comparisons of Position-Time Profiles for Two Similar Test Runs and the XMF and XSF Data for a Given Test Run

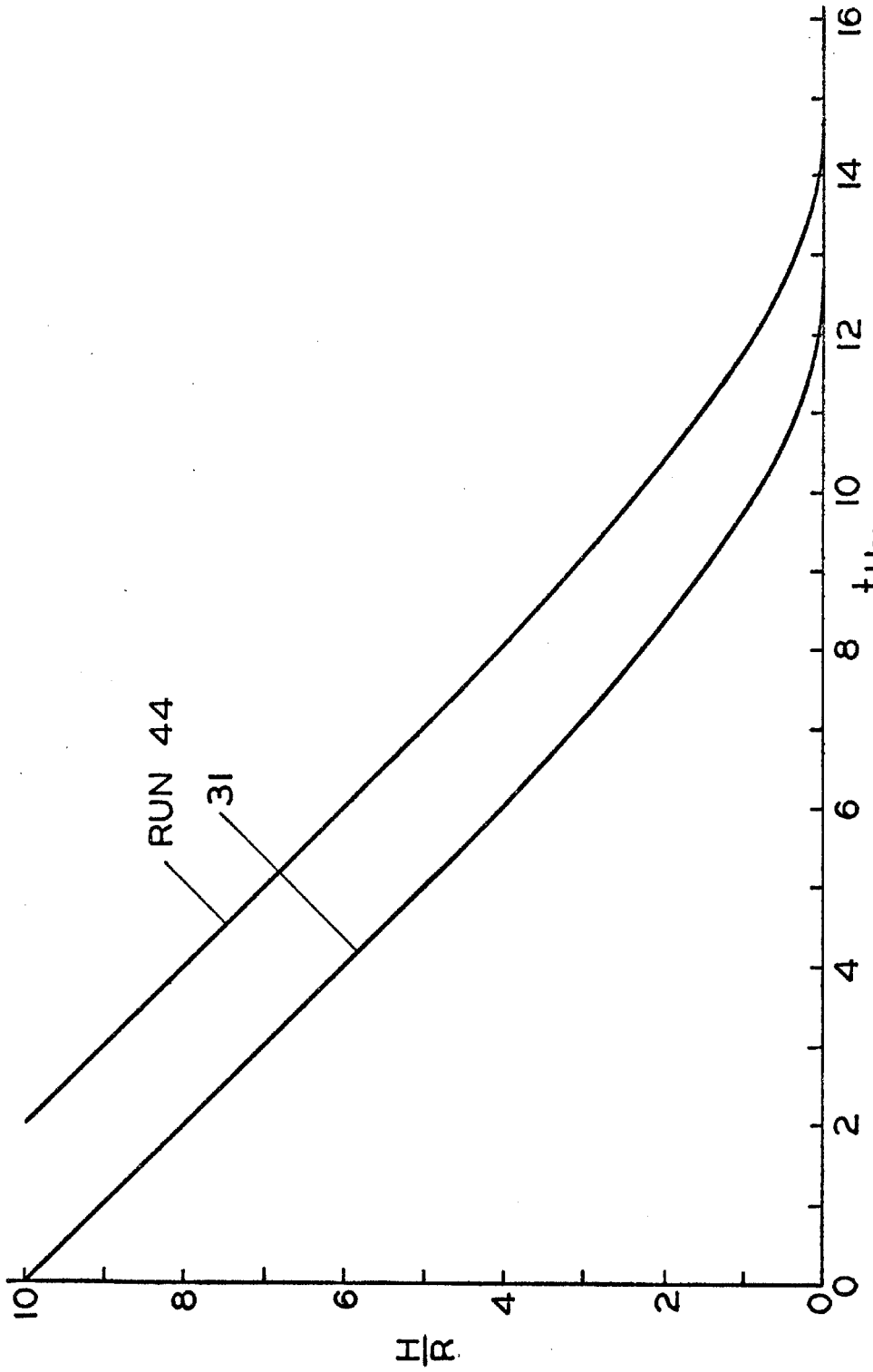

Figure 14. Comparison of Position-Time Profiles for Similar Terminal Reynolds Numbers

diameter of the ball used in run 31 was twice that used for run 44, while the Reynolds number differed by 8 per cent (see Appendix C).

The interpretation of the position-time profile for the lowest Reynolds number case recorded (runs 21, 22; Re_T O(.05)) is relatively straightforward. At this Reynolds number, the ball is in the "creeping flow" regime, for which the correct length scale is the radius R. The velocities are low enough throughout the profile that the kinetic energy of the particle is always small compared to its potential energy. Thus, the position plot represents a good approximation to the energy plot within a constant. The rate of energy loss begins to increase at $H/R \approx 8$ and rapidly increases below $H/R \approx 3$. (Note: since both XMF and XSF will be used in this section, let the height of the ball bottom above the floor plane be characterized by H.) At a position 8 radii ahead of the leading edge of an advancing ball in an infinite fluid, the Stokes solution gives a fluid velocity equal to 17 per cent of the ball velocity; 3 diameters ahead, a fluid velocity equal to 37 per cent of the ball velocity[13]. Thus, the energy loss rate is accelerated as the Stokes flow field surrounding the ball interacts with the floor plane. A detailed description of this process applicable when the sphere is more than approximately 1/4 of a radius from the wall is given in Happel and Brenner[14].

As a measure of the decrease of this length scale with increasing Reynolds number, the approximate point on each profile at which the particle kinetic energy was one-third of the kinetic energy at terminal velocity was located. The rate of change of velocity with height is so small that it was hard to locate the point exactly, but the

trend was clear. Figure 15 presents these data as a function of Re_T. It appears from this graph that even for a Reynolds number as low as 10 the major energy loss is concentrated during the last fraction of a ball radius of approach to the floor.

The presence of particle rebound was first observed at a Reynolds number of 25.6 and verified at 27.9 with a different ball diameter. The highest Reynolds number for which a rebound did not occur was 13.5.

The per cent momentum recovery was chosen as the measure of the collisional losses. The scatter of the data near the bounce point, and the shape of the rebound position curve as kinetic energy was transformed into potential energy, limit the accuracy of the measurement, but again, the trend is clear. Figure 16 is presented to show the increase in momentum recovery as the Reynolds number is increased. The ends of the bracket locate two readings: the best value based on XMF data and the best value based on XSF data. It does not show the possible error range (which is considerable) for the measurements. The value of this curve is to show the data trend toward greater momentum recovery as the Reynolds number is increased.

The per cent momentum recovery is limited by losses associated with the interaction of the ball and the steel anvil. Air drop tests (see Part II) were run with clean balls being dropped on the dry anvil. A plot of rebound height as a function of initial drop height showed a constant per cent energy recovery over a range of impact velocities up to 200 cm/sec. The energy recovery varied slightly with ball di-

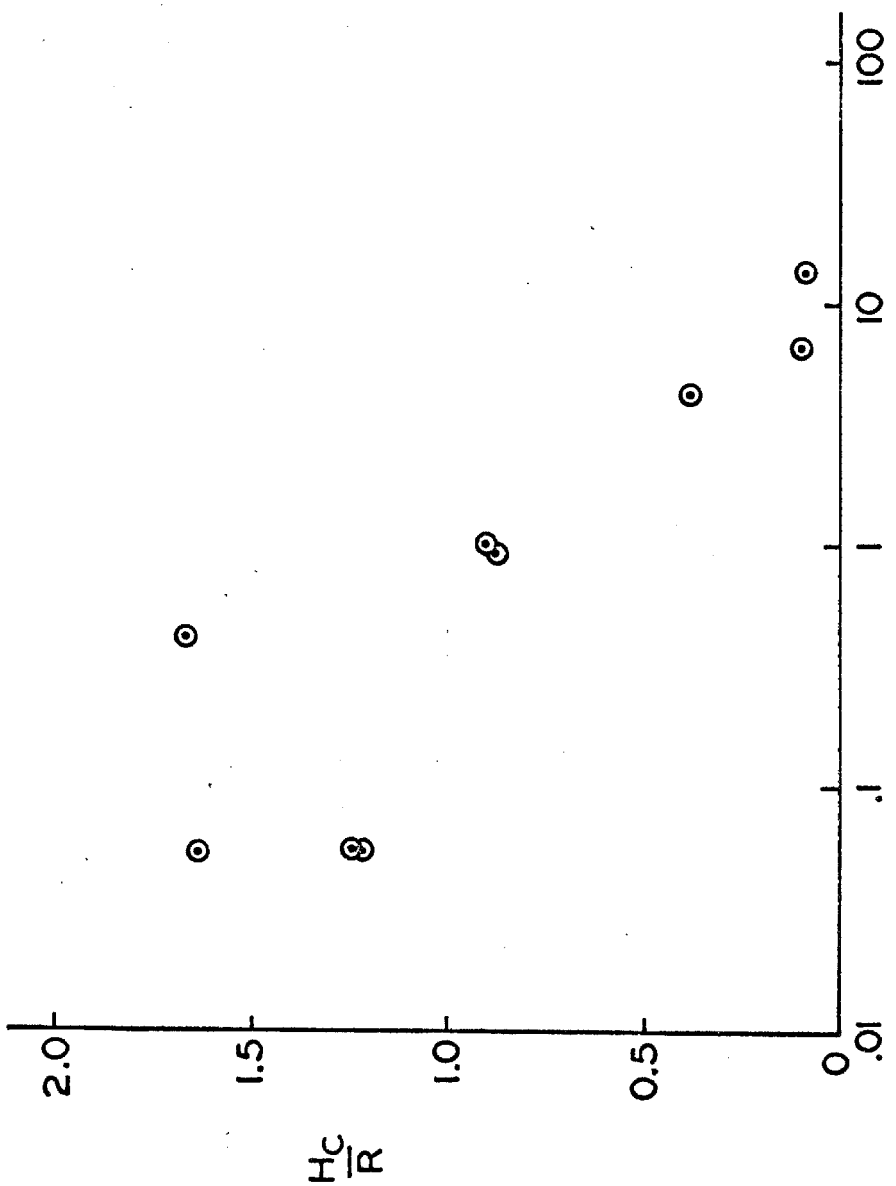

Figure 15. Height Above Rebound Surface (H_c) at Which the Particle Kinetic Energy Has Been Reduced by Two-Thirds

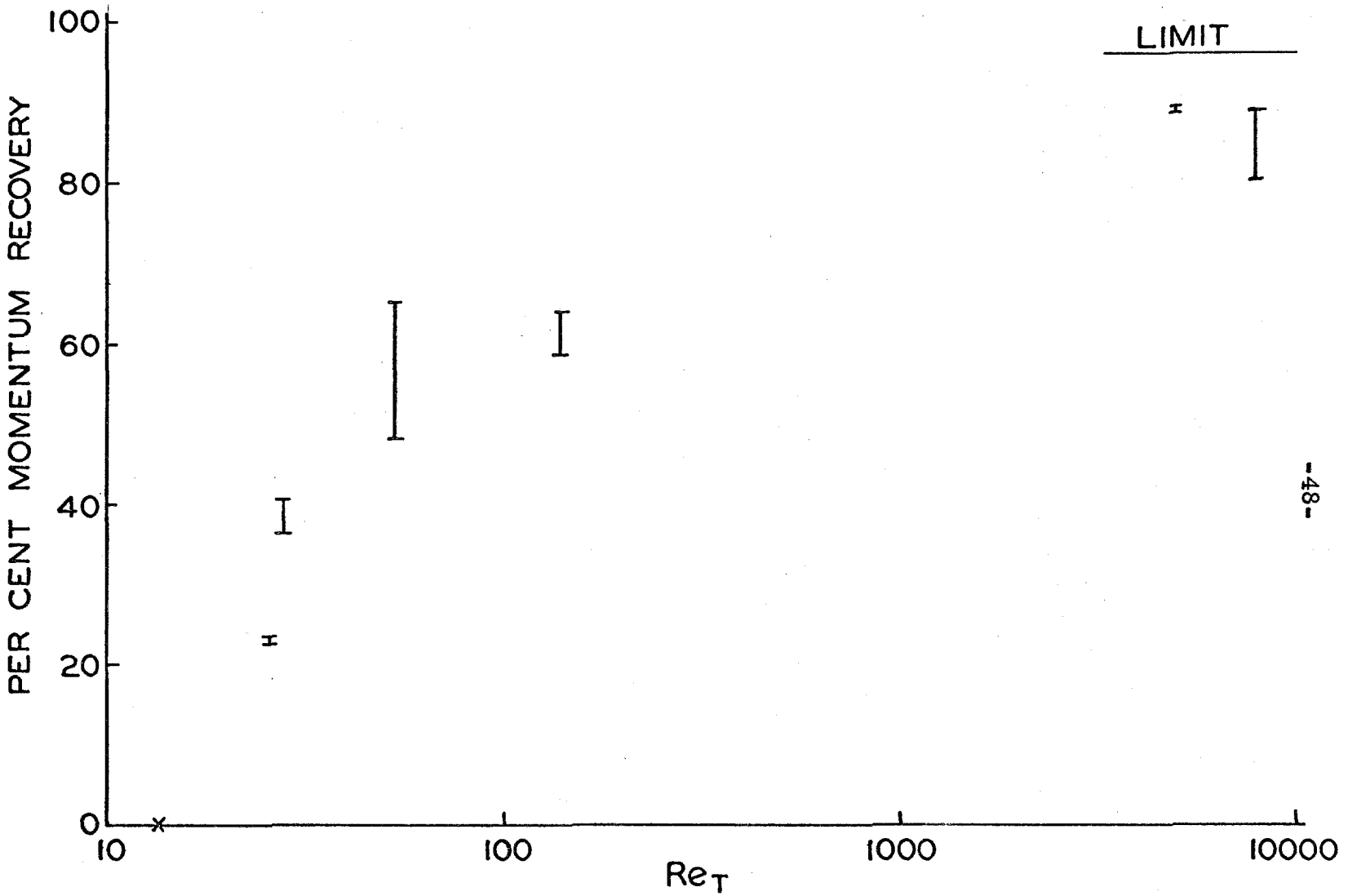

Figure 16. Per Cent Particle Momentum Recovery Upon Rebound

ameter. An attempt was made to verify this behavior analytically. The energy loss (2 - 4 per cent) could not be accounted for in the form of elastic vibrations in the anvil. Hunter's[15] analysis, based on Hertz stresses, assumed no plastic deformation and gave a particle energy loss an order of magnitude smaller than the observed loss. An analysis by Zener[16] assumed the displacement of the anvil surface to be proportional to the impulse from the sphere over the area of contact. The results of this analysis showed that the deviation from perfect restitution should vary (for our data) as the impact velocity to the one-fifth power or the drop height to the one-tenth power. Thus, our straight line fit (constant per cent energy restitution) should be good over the limited range of velocities considered. The correlation based on ball radius did not fit as well, but this was attempted with limited data.

The per cent momentum recovery measured on the dry anvil was 96.8 for 0.3175-cm balls and 98.1 for 0.635-cm balls. Since the highest Reynolds number case was recorded using a 0.635-cm ball, its maximum recovery value is plotted on Figure 16. Note that as Re_T increases, the per cent momentum loss due to the fluid mechanics of the problem decreases, until it is of the order of magnitude of the losses due to the solid mechanic interactions of the particle and the anvil. The heavy particles have so much kinetic energy that the viscous interactions with the wall have only a small relative effect on the total energy.

The absence of data between the Reynolds numbers of 138 and 4950 is due to a peculiarity of the flow field. Runs were tried at Re_T

of 200 and 440 with ball diameters of 0.635 cm and 0.9525 cm, respectively. In both cases, the ball fell in a very erratic manner, sometimes moving several inches off the tank centerline. This Reynolds number range corresponds roughly to the region of growth, oscillation, and shedding of the ring vortices in the ball wake[2]. These tend to produce unbalanced lateral forces on the ball and cause the erratic motion. It was at this point in the study that the decision was made to discontinue testing and to use the high Reynolds number data obtained in the preliminary studies.

As a further verification of the thin-film energy loss mechanism, an experiment of a completely different type was run. What was attempted was a duplication of the energy loss of run 16 (Re_T = 7870) using a very thin water film. An aluminum retaining ring was built to rest on the top of the anvil to contain a liquid film on the rebound surface. A hypodermic needle was used to measure small volumes of distilled water. The tests were run in the same manner as the air drop tests to determine the dry anvil energy losses. The ball drop height was chosen to give a modified Reynolds number approximately equal to the terminal Reynolds number of the continuum tank test. The modified Reynolds number was based on the fall velocity as it entered the liquid film, the ball diameter, and the density and viscosity of the film liquid. The motivation was that then the Reynolds number of the ball as it entered this high-loss zone was matched for the two cases.

To show the thin film effect, the test was run at five different film thicknesses from 0.50 mm to 1.67 mm. The previously deter-

mined dry anvil data point was also used. Figure 17 shows the results of this test along with the data from continuum test run 16. The average reading is marked along with an error band to show the maximum scatter of the data. The energy loss increases rapidly as the film thickness increases from zero and then begins to level off. This indicates that beyond a certain film thickness the increase in the film thickness does not contribute much to the total energy loss. This is strong evidence for the thin-film energy loss hypothesis. The data for continuum run 16 (infinite film thickness) show a 2.2 - 11 per cent lower energy loss than the loss for the thickest film used. Further testing will be required to verify the shape of the loss curve for other Reynolds numbers and to investigate this difference in energy loss between the two tests. Regardless of the differences, the fact that the loss curve has a definite break in it tends to verify the thin-film energy loss mechanism for this condition.

Several effects which separately appeared small could have contributed to the energy loss difference between the two tests. No estimate was made of the energy lost to the splash effect in the thin film. Also, no test was made to determine the additional rebound mass due to water adhering to the sphere surface. Further experiments are suggested in order to get a firm estimate of these losses.

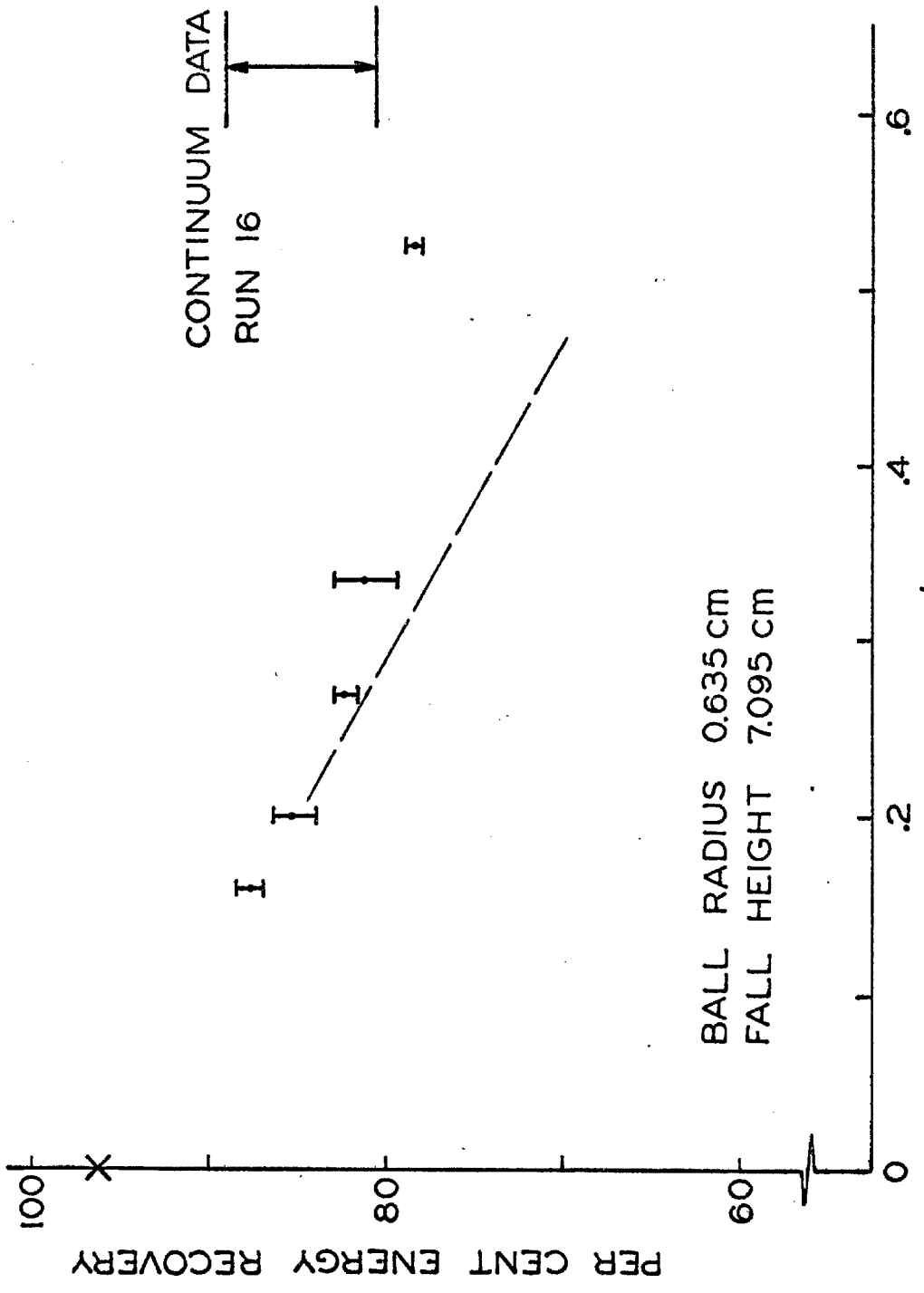

Figure 17. Thin-Film Test Energy Recovery Results

VI. CONCLUSIONS

The stated purpose of this study was to investigate the effects of particle-particle interactions on the momentum transfer process in liquid-particle two-phase flows. The subsequent simplification of basic geometry diminishes the applicability of the actual numbers obtained in this study to flows of interest. The trend and order of magnitude of the results, however, should be representative of the processes occurring in two-phase flow. All numbers quoted below refer to the experimental geometry.

The results showed two definite flow regimes. For Re_T less than about 20, the particle kinetic energy was dissipated in approaching the wall and no rebound occurred. Above $Re_T \approx 10$ it appeared that over 2/3 of the energy dissipation occurred within a tenth of a radius of the wall.

At higher Re_T, the sphere rebounded from the wall. As Re_T was increased, the loss became a smaller fraction of the incoming terminal kinetic energy. At $Re_T \approx 5000$, the loss had been reduced to approximately 11 per cent.

Thus, all of the experimental results point to a thin-film energy loss mechanism over a wide range of Re_T. Note also that if the data correlated based on $Re(\rho_s/\rho)$ as suspected, then for gas flows with the density ratio of $O(10^3)$, the "critical Reynolds number" would be decreased by a factor of $O(10^2)$.

These results motivated a different energy loss experiment utilizing a thin liquid film. The results of this test showed that a

critical film thickness existed, above which the energy loss did not significantly increase with increasing thickness. The critical thickness for the case chosen was approximately one-fifth of a ball radius. Further testing is required to attempt a correlation of the energy losses for the two separate experiments.

REFERENCES

1. Torobin, L. B. and Gauvin, W. H., "Fundamental Aspects of Solids - Gas Flow," Can. J. of Chem. Eng. (in 5 parts), 37, 129, 167, 224 (1959), and 38, 142, 189 (1960).

2. Hoglund, R. F., "Recent Advances in Gas - Particle Nozzle Flows," J. Am. Rocket Soc., 32, 662 (May 1962).

3. Marble, Frank E., "Dynamics of a Gas Containing Small Solid Particles," Proceedings of the 5th AGARD Colloquium, 1963, pp. 175-213, Pergamon Press, Oxford (1963).

4. Marble, Frank E., "Mechanism of Particle Collision in the One-Dimensional Dynamics of Gas - Particle Mixtures," Phys. Fluids, 7, 1270 (1964).

5. Rannie, W. D., "Perturbation Analysis of One-Dimensional Heterogeneous Flow in Rocket Nozzles," Progress in Astronautics and Rocketry: Detonation and Two-Phase Flow, Vol. 6, pp. 117-144, Academic Press, New York (1962).

6. Marble, Frank E., "The Role of Approximate Analytical Results in the Study of Two-Phase Flow in Nozzles," Proceedings of the Air Force Rocket Propulsion Laboratory Two-Phase Flow Conference, 15-16 March 1957, San Bernardino, California, AFRPL-TR-67-223, Vol. II (August 1967).

7. Murray, J. D., "Some Basic Aspects of One-Dimensional Incompressible Particle - Fluid Two-Phase Flows," Astronautica Acta, 13, 417 (1967).

8. Moorman, R. W., "Motion of a Spherical Particle in the Accelerated Portion of Free Fall," Ph. D. Thesis, State University of Iowa (1955).

9. Sheely, M. L., "Glycerol Viscosity Tables," Industrial and Engineering Chemistry, 24, 1060 (1932).

10. Bosart, L. W. and Snoddy, A. O., "New Glycerol Tables," Industrial and Engineering Chemistry, 19, 506 (1927).

11. Handbook of Chemistry and Physics, 41st Edition, pp. 2129, 2181, Chemical Rubber Publishing Company, Cleveland (1959).

12. Lindgren, B. W. and McElrath, G. W., Introduction to Probability and Statistics, The Macmillan Company, New York (1959).

13. Lamb, H., Hydrodynamics, p. 598, Dover Publications, New York (1945).

14. Happel, J. and Brenner, H., Low Reynolds Number Hydrodynamics, pp. 329-332, Prentice-Hall, Inc., Englewood Cliffs, N. J. (1965).

15. Hunter, S. C., "Energy Absorbed by Elastic Waves During Impact," J. Mech. Phys. Solids, 5, 162 (1957).

16. Zener, C., "The Intrinsic Inelasticity of Large Plates," Phys. Rev., 59, 669 (1941).

APPENDIX A

Continuum Test Preparations and Procedure

I. Preparation of Equipment

A. Cleaning

1. Anvil:

The anvil was washed with M-6 (oxylene solvent) and methanol.

2. Interior tank walls:

Tank walls were cleaned with plastic cleaner, then scrubbed and flushed with distilled water.

3. Steel balls:

These were soaked in M-6 (oxylene solvent) to remove the grease coating, soaked and agitated in methanol, rubbed with Kimwipe tissues, and air dried.

4. Electromagnet:

The electromagnet was cleaned with methanol and air dried.

B. Preparing Solutions

1. Initial solution:

The tank was filled with undiluted glycerin direct from the drum. The solution remained undisturbed for two days, during which time most of the bubbles present initially disappeared; the bubbles remaining were removed using a plexiglass rod.

2. Subsequent solutions:

Both distilled water and glycerin were added. In all cases, the glycerin concentration was being reduced, but additional glycerin was sometimes needed to provide the

liquid depth required for the particle to reach terminal velocity. These additions and subsequent stirring produced many bubbles. Over a period of no less than 36 hours, the mix was stirred intermittently until a true solution was obtained. It was obvious when this condition was approached: when the solution was not thoroughly mixed, stirring produced obvious density striations; when little or no evidence of these striations was present, the solution was allowed to stand overnight before the series of test runs was performed.

C. Preparation of Tank Equipment

A plexiglass rod with a 3-inch flat section glued to the end was used to sweep the anvil clear of any small particles that had settled there. This procedure also served to mix the solution and to reduce any temperature gradients present in the tank.

D. Preparation of Camera and Related Equipment

1. Camera speed:

The speed was chosen from preliminary analyses (which gave the anticipated ball velocities) to give sufficient resolution and sufficient full-speed run time.

2. Lens aperture:

The aperture was chosen from 1. above and preliminary test lighting data.

3. Focusing:

The camera was focused on a 2-inch high, 1-inch wide piece of angle using a ground surface focusing strip. The angle was placed off to the side and at the mid-plane of the anvil with a marked face toward the camera. This proved to be a very sensitive technique.

4. Camera and lights:

The previously determined lens aperture and framing speed were set and the position of the lights checked.

II. Description of Test Procedure

A. Arranging Electromagnet

The electromagnet was cleaned and placed in the tank at the appropriate height above the anvil.

B. Sampling Test Liquid

A clean 125 ml beaker was taped to a clean plexiglass rod and then lowered into the tank. The beaker was then moved to a position near the bottom of the tank. Approximately one-third of the sample was obtained as the bottle was lowered through the liquid, and the remaining portion with the beaker opening approximately 5 inches from the anvil top. When the beaker was filled, it was removed from the tank and a plastic screw cap was affixed.

C. Positioning Ball

To put the ball on the electromagnet, the magnet was raised to the level of the tank top by raising the magnet holder piece through a locating sleeve in the support. The DC current level (0.05 - 0.15 amps) was established and the ball was transferred to the magnet using a tweezers. The magnet was then lowered into the test position and the location pin in the support was put in place.

D. Preparing Film and Camera

The film was loaded in the camera, after first removing and boxing the film, if any, from the previous run.

E. Adjusting Final Details

Approximately five minutes after the ball was lowered into the tank, and at least fifteen minutes after the liquid sample was

taken, the final adjustments were made. The camera was put into 'run' condition; lights were turned on to the correct level; the camera was started.

F. Dropping Balls

Following an appropriate time lag after the camera was started, the electromagnet was switched from DC to AC power, causing the ball to drop.

G. Preparing for Next Run

To minimize the time between runs, the step causing the most test liquid motion was performed first. This step was to remove the ball from the tank with a small permanent magnet attached to a 1/4-inch plexiglass rod.

H. Recording Data

The time, the two tank temperatures, and the room temperature were recorded.

I. Completing Test Run Series

The above cycle, starting with II C above, was then repeated for all test runs at one glycerin concentration. The tank was covered with a sheet of plastic between series of runs to keep out dust and to restrict the absorption of water by the hygroscopic solution.

J. Recording Final Data

After the final test of each series, the positions of the electromagnet, the thermometers, and camera were recorded.

APPENDIX B

Fluid Property Determination Procedures

I. Equipment

A. Specific Gravity Bottles

Two specific gravity bottles, having nominal capacities of 25 and 50 ml respectively. Stopper with capillary tube and ground glass sealing surface. Cap to retard evaporation.

B. Viscosimeter

Hoeppler falling-ball viscosimeter, Model HV 303.

C. Constant-Temperature Bath

A 5-gal jar, open on top, sides covered with 1-inch thick layer of fiberglass insulation enclosed in aluminum foil.

D. Bath Control

Precision Scientific Company Porta-Temp to heat and stir bath, and pump bath water through viscosimeter.

II. Preparation

A. Room temperature adjusted to less than test temperature, 25°C.

B. Test sample cooled to 10°C in refrigerator.

C. Bath cooled to 20°C using tap-water cooling coil.

D. Specific gravity bottles and viscosimeter cleaned with distilled water and methanol.

E. Bottles and viscosimeter filled with sample solution.

F. Bottles shaken and tapped on laboratory table to dislodge bubbles. Capillary tube cap with ground glass sealing surface inserted.

G. Viscosimeter arm rotated to dislodge bubbles. Plastic rod used if needed. Tube sealed.

H. Bottles inserted into pan suspended in water bath.

III. Test

A. By hand control of heater, bath temperature raised from 20°C to test temperature, 25°C, over 30 minute interval.

B. Temperature maintained at test temperature (±0.08 °C) for 20 minutes. Arm of viscosimeter rotated periodically to reduce possible temperature gradients. Excess fluid in specific gravity bottles wiped from top of capillary tube.

C. Specific gravity bottles removed from bath; exteriors cleaned with methanol; bottles capped.

D. Three to five viscosimeter runs performed to get average falling time of viscosimeter ball.

E. Specific gravity bottles weighed on precision single-pan balance to ± 0.0005 gms.

APPENDIX C

Measured and Calculated Test Conditions

Run Number	Solution Designation	Ball Diameter (cm)	Solution* Density (gm/cc)	Solution* Viscosity (poise)	Terminal Velocity (cm/sec)	Terminal Reynolds Number, Re_T	$(\frac{\rho_s}{\rho})Re_T$
16	W	0.6350	0.9974	0.00925	115.0	7874	61420
19	W	0.4763	0.9974	0.00925	96.38	4950	38610
21	A	0.2381	1.2667	10.68	1.93	0.055	0.34
22	A	0.2381	1.2666	10.66	2.02	0.057	0.35
28	A	0.3969	1.2665	10.48	6.64	0.319	1.96
31	A	0.6350	1.2665	10.45	13.19	1.015	6.24
36	A	0.9525	1.2663	10.28	27.05	3.174	19.5
44	B'	0.3175	1.2529	3.76	8.92	0.944	5.86
46	B	0.6350	1.2517	3.35	28.34	6.724	41.8
52	C	0.6350	1.2460	2.39	40.66	13.46	84.0
56	C	0.9525	1.2459	2.39	56.19	27.90	174.2
66	D	0.6350	1.2364	1.39	45.31	25.59	161.0
71	E	0.6350	1.2258	0.802	54.63	53.02	336.5
76	E	0.9525	1.2258	0.804	94.73	137.6	873.3

* At test temperature.